Feldspathic Clasts in Yamato 86032: Remnants of the Lunar Crust with Implications for Its Formation and Impact History.

L. Nyquist[1], D. Bogard[1], A. Yamaguchi[2], C.-Y. Shih[3], Y. Karouji[4], M. Ebihara[2,4], Y. Reese[5], D. Garrison[3], H. Takeda[6]

[1]Mail Code KR, NASA Johnson Space Center, Houston, TX 77058

(laurence.e.nyquist@nasa.gov)

[2]National Institute of Polar Research, Department of Polar Science, Graduate University of Advanced Studies, Tokyo 173-8515, Japan

[3]Mail Code JE-23, ESCG/Jacobs Sverdrup, Houston, TX 77058

[4]Graduate School of Science, Tokyo Metropolitan University, Tokyo 192-0397, Japan

[5]Mail Code JE-23, ESCG/Muniz Engineering, Houston, TX 77058

[6]Research Institute, Chiba Institute of Technology, Narashino 257-0016, Japan.

Abstract

Yamato (Y)-86032 is a relatively large, feldspathic lunar highlands meteorite composed of a variety of highland lithologies. Low bulk contents of Th and Fe indicated that it came from a region of the moon far distant from the Procellarum KREEP Terrain (PKT) and the Apollo landing sites, perhaps from the farside. A large (5.2 x 3.6 cm) slab was cut from Y-86032 . We report results from coordinated textural, mineralogical-petrological, chemical, and isotopic studies of lithologies identified in the slab, emphasizing the results of ^{39}Ar-^{40}Ar, Rb-Sr, and Sm-Nd chronological studies as well as Sm-isotopic studies. These studies characterize the history of Y-86032 and its precursors in the farside mega-regolith, leading to inferences about the formation and evolution of the lunar crust.

Textural studies establish that theY-86032 breccia is composed of a variety of highland components including feldspathic breccias, and other components, such as possible VLT mare basalts. Impact melt veins smoothly abut the other lithologies. Thus, Y-86032 experienced at least two impact events. These impacts occurred on a predominantly feldspathic protolith, which formed 4.43±0.03 Ga ago as determined from a Sm-Nd isochron for mineral clasts separated from the two dominant lithologies. Initial ^{143}Nd/^{144}Nd in the protolith at that time was -0.64±0.13 ε-units below ^{143}Nd/^{144}Nd in reservoirs having chondritic Sm/Nd ratios, consistent with prior fractionation of mafic cumulates from the LMO. Although the mineral chemistry of these clasts differs in detail from that of minerals in Apollo 16 Ferroan Anorthosites (FANs), the Rb-Sr studies establish that the initial ^{87}Sr/^{86}Sr in them was the same as in the FANs. This observation implies a single Sr-isotopic composition for farside and nearside terrains during lunar crustal formation. An ^{39}Ar-^{40}Ar age of a feldspathic breccia clast of 4.38-4.41±0.035 Ga strongly supports an old igneous formation age for the farside terrain, whereas an ^{39}Ar/^{40}Ar age of 4.10±0.02 Ga for a second feldspathic breccia clast records the time of a major impact event in the farside highlands. Interpretation of the ^{39}Ar-^{40}Ar data for a sample of impact melt cross-cutting the two major lithololgies of the breccia; i.e., the feldspathic breccia and a dark regolith breccia, is complicated by trapped solar wind and lunar atmosphere ^{40}Ar. Analysis of the dark regolith breccia itself, combined with previously estimated ^{40}Ar/^{36}Ar = 10 for the moon at ~4 Ga ago, implies melt formation and final breccia assembly at

~3.9 Ga ago. None of the breccia lithologies were exposed to thermal neutron fluences exceeding ~2 x 10^{15} n/cm^2, only about 1% of the fluence experienced by some other lunar highlands meteorites. Thus, Y-86032 spent most of the time following final brecciation deeply buried in the megaregolith. Cosmic ray exposure ages of ~3-8 Ma verify that the lunar surface exposure of Y-86032 was short, in agreement with the neutron fluence data. This study further demonstrates that the original crystallization ages of lunar crustal rocks and the time of individual impact events can be reliably recorded in rocks from the megaregolith, and were not necessarily obliterated by impact reworking of the lunar crust.

1. INTRODUCTION

Lunar meteorites of predominantly feldspar composition offer a much broader sampling of the early lunar crust compared to Apollo-returned rocks, and almost certainly include material from the farside highlands. Consequently, such rocks may yield additional insights into early lunar history. Yamato (Y)-86032 is a large (648 gram) feldspathic lunar highland meteorite. It is a breccia composed of a variety of highland lithologies (Takeda et al., 1989, Koeberl et al. 1989, Takeda et al., 1990; Palme et al., 1991; Yamaguchi et al., 2004). One ancient feldspathic clast has an Ar-Ar age of 4.35-4.41 Ga (Bogard et al., 2000), and Sm-Nd isotopic systematics implying negative ε_{Nd} at that time (Nyquist et al., 2002), suggesting a direct link to the primordial lunar magma ocean (LMO). The low contents of Th and Fe indicate that Y-86032 comes from a region of the moon that is far distant from the Procellarum KREEP Terrain (PKT) and the Apollo landing sites, perhaps from the farside of the Moon (Takeda et al., 1990; Yamaguchi et al. 2004; Karouji et al., 2004). Thus, Y-86032 provides us with an opportunity to study highland lithologies not sampled by the Apollo and Luna missions. Although other lunar meteorites may also come from the lunar farside, the uniquely low Th and Fe contents of Y-86032 make the argument for a farside origin of Y-86032 particularly strong. Additionally, as we will discuss in this paper, its low cosmic ray exposure age (~8 Ma), and the low thermalized secondary neutron fluence in its clasts and impact melt matrix suggests that it remained shielded by several meters of megaregolith throughout its history. This likely combination of lunar-farside and deep-megaregolith origin makes Y-86032 an extremely important, if complicated, lunar sample. We thus undertook a comprehensive combined mineralogical/petrographic, chemical, and chronological study of Y-86032 in order to better elucidate its history. Additional information about Y-86032 obtained by earlier consortium studies can be found in Takeda et al. (1989) and Koeberl et al. (1989), and in later issues of the proceedings of NIPR symposia on Antarctic meteorites. Preliminary reports of the work presented here were given by Nyquist et al. (2005) and Yamaguchi et al. (2005).

2. SAMPLING: TEXTURAL RELATIONSHIPS AND MINERALOGY (Small Type)

A slab (5.2 x 3.6) cm^2 x 3-5 mm thick was cut through the center of the meteorite (Fig. 1). A separate paper describing the detailed texture, mineral chemistry, and bulk chemistry of slab lithologies is in preparation. Here we give a brief summary of those data to aid interpretation of the isotopic data that are the focus of this paper. We identified white (W) (~5 vol%), light gray (LG) (~20 vol%), dark gray (DG), and impact melt (IM) lithologies in the slab. The textural relationships among these lithologies for the portion of the slab within the outline in Fig.1 are shown in Fig.2. Here it is seen that a fragment of the LG lithology was broken away and surrounded by the DG lithology during the brecciation event that joined them. Note also that the IM lithology smoothly abuts both of the other lithologies. W- and LG-clasts occur scattered throughout both the DG and IM lithologies. The LG lithology is itself brecciated, which may have occurred either prior to the joining of the LG- and DG-lithologies, or during that event. The breccia is well-lithified and has very low porosity.

Subsamples of the distinct lithologies were separated by a chisel for allocation for the analyses reported here. Note that samples from the earlier consortium studies were separated from ~4 cm away from our slab. Preliminary results from earlier studies of a light-colored clast were reported by Bogard et al. (2000), Takeda et al. (2002), and Nyquist et al. (2002). New samples representing the three main lithologies in the slab (LG, DG, and IM) were allocated for this study. The sample studied by Bogard et al. (2000) and Nyquist et al. (2002) was identified as a “Gray Clast” extracted from the allocated sample ,116 and was designated as ,116 GC. The characterization of the clast types as “white” or “gray” is somewhat subjective, as the coloration is gradational. The earlier petrographic study by Takeda et al. (2002) accompanying the isotopic studies of Bogard et al. (2000) and Nyquist et al. (2002) were of Polished Thin Section (PTS) 83-1 identified as containing part of the same clast contained in ,116. Samples Y-86032,116 and 117 were produced from ,52, which is a remainder after separation of ,82 and ,83. All of these samples are from the original ,20, which contained a large ”light” clast shown in Fig. 1 of Takeda et al. (1989). The largest white clast in ,20 was separated as ,82 and the smaller one as ,83. The chip ,82 was studied by Tatsumoto and Premo (1991) and Takaoka and Yosida (1992). The remainder was ,52, and appeared to also include a part of the large clast. PTS Y-86032,83-1 was found to

contain three major lithologies: a light-colored feldspathic breccia clast, fragmental breccia matrices rich in mafic minerals, and fragment-laden dark glassy breccia (Takeda et al., 2002). It also is possible that ,116 GC was an example of what is termed here the white (W) lithology, occuring as individual mm-sized clasts throughout the meteorite. As discussed later in the paper, the ,116 GC clast has a somewhat older Ar-Ar age than another light-colored feldspathic breccia clast, LG ,28, but experienced the same thermal neutron fluence as LG ,28. It is probable that the W and LG lithologies are closely related, with indvidual clasts being distinguished by the degree of shock and thermal metamorphism they experienced during the brecciation process.

To insure close correlation between the petrographic and isotopic studies of this investigation, eight PTSs were made from representative portions adjacent to the samples used for chemical and isotopic studies, and were examined by optical microscope, a scanning electron microscope (SEM) (JEOL 5900 LV), and an electron microprobe analyzer (EPMA) (JEOL JXA 8800) at the National Intitute of Polar Research (NIPR), Tokyo. The bulk chemistries of the lithologies were analyzed by instrumental neutron activation analysis (INAA) and inductively coupled plasma mass spectrometry (ICP-MS) at Tokyo Metropolitan University (TMU). A preliminary report of the chemical data was given by Karouji et al. (2004). More detailed reports of the results of the mineralogical-petrological and chemical studies are in preparation.

2.1 Texture and mineral chemistry

The W lithology occurs as rounded or subrounded clasts (up to 3 mm in size) of anorthosite with minor mafic minerals (<1-5 vol%). It includes a variety of feldspathic clasts such as feldspar fragments, granulitic clasts and clasts similar to white portions in the LG lithology.

The LG lithology is a breccia mostly composed of fragments of anorthosite (94.5%) with minor amounts (~5%) of pyroxene, olivine, silica minerals, and chromite. Olivine compositions are mostly $Fo_{78.1-82.4}$, but there are some relatively Fe-rich olivine grains ($Fo_{66.4-64.6}$). The compositions of pyroxene vary significantly: low-Ca (<5 mol% Ca) pyroxenes have mg' (= Mg/(Mg+Fe) x 100) = 41.0-81.3.

Plagioclase compositions range from $An_{\sim 85.4}$ to $An_{\sim 96.6}$ with two peaks at $An_{\sim 88.5}$ and $An_{\sim 93}$. There is a grain of AlMg-chromite ($Usp_{2.2}Sp_{42.5}$) (mg'=41.6). We also found a moderately brecciated clast, composed of plagioclase ($An_{88.9}$) and Fe-rich augite grains ($Wo_{39-4}En_{31-39}$) (<0.2 mm in size). The augite grains have fine planar exsolution lamellae of low-Ca pyroxene. On the An versus mg' diagram, this clast plots outside the regions of pristine nonmare rock groups, probably forming a different suite of igneous rocks (Yamaguchi et al., 2004). The LG lithology may be composed of fragments from augite-bearing anorthosites with plagioclase of ~$An_{88.5}$ plus anorthosites with more An-rich plagioclases and more Mg-rich mafic minerals. The rocks thus represented may form a single suite of igneous rocks.

The DG lithology is a dark matrix composed of a variety of clast types: fragments of feldspathic clast (W lithology), glassy (impact melt) clast , granulitic clasts, basaltic clasts, and mineral fragments. Olivine compositions vary from $Fo_{8.7-83.3}$, and the mg' of pyroxenes varies in the range 38.3-81.2. Plagioclase compositions are $An_{68.8-97.9.}$ On the An versus mg' diagram, two granulitic clasts plot between the FAN and Mg-suite fields, like those found in the Apollo granulites (Lindstrom and Lindstrom, 1986). The basaltic clast (0.40 x 0.38 mm in size) is composed of plagioclase and pyroxene with minor amounts of silica minerals and Ti-rich phases in the DG lithology. The pyroxenes are widely zoned ($Wo_{4.7}En_{71.3}$-$Wo_{24.5}En_{14.8}$) and show a strong correlation between Fe/(Fe+Mg) (Fe#) and Ti/(Ti+Cr) (Ti#), overlapping the range of VLT basalt (Nielsen and Drake, 1978). There are also fragments of mafic minerals that could be derived from mare basalts. The grain boundaries of clasts and mineral fragments are cemented by very fine vesiculated intergranular melts.

The IM vein is a dark glassy matrix with various kinds of lithic and mineral fragments similar to those in the DG lithology. The textural observations suggest that Y-86032 is a breccia resulting from at least two impact events. At the first event, the LG breccia was incorporated into the DG matrix, and at the second event both lithologies were shear-deformed and cut by IM veins. Since the LG-lithology is itself brecciated, a third, prior impact event also may have occurred. The presence of vesiculated intergranular melts in the DG lithologies suggests peak shock pressures of ~10-15 GPa (Bischoff and Stöffler 1992). The temperatures were locally more than ~1600°C, but the bulk temperatures were no

more than several hundreds of °C judging from the small amounts of melts. The breccia was shocked again after initial formation, and impact melt veins (~20-30 vol%) formed locally. After thermal equilibration, the bulk temperature would have increased to >400°C. These shock events could have partially reset some of the Ar-Ar ages. As shown below, the range of Ar-Ar ages of the lithologies implies at least two and possibly three impact heating events.

3. CHEMICAL COMPOSITION OF THE Y-86032 LITHOLOGIES

3.1 Bulk chemistry

The chemical data for the slab samples are mostly consistent with previous data for Y-86032 (Palme et al., 1991; Koeberl et al., 1989; Korotev et al., 1996), except for Na, Al, V, Cr, Mn, and HREEs. The FeO content of the LG breccia (2.37 wt%) is lower than that of other lunar highland meteorites (Korotev et al., 1996). The Na/Ca and Fe/Mg ratios reflect the degree of geochemical evolution. Na/Ca in LG is higher than in DG and IM, while Fe/Mg in LG is lower than in the other lithologies. Also, the abundance of REEs in DG and IM are similar to values obtained in previous analyses of Y-86032, but those in LG are lower (x 0.5-0.6 except Eu) (Fig. 3). This may be due to contributions of minor basaltic components in DG and IM, as indicated by the textural observations.

The contents of Fe, Mg, and REEs in the DG matrix are clearly higher than those of LG and FAN, consistent with the previous bulk data of 'matrices' of Y-86032, e.g., Koeberl, et al. (1989). Thus, this is unlikely to be due to sample heterogeneity (i.e., oversampling of orthopyroxene). Instead, it could be due to the presence of minor components such as VLT basalts and/or other highland components.

3.2 Igneous components of the breccia

We applied a mixing model with two endmenbers, LG and VLT basalts, to the DG composition. In this model, the composition of LG is used as a proxy for the composition of ferroan anorthosites (FANs) because it lies within the range of FAN compositions except for a few elements such as Na. We assumed that the elevated abundances of REEs, Fe, and Mg of DG compared to those of LG were due to the presence of VLT basalts similar in composition to those found by Lunar 24 (Warren and Kallemeyn

1989). To explain the elevated FeO abundances (5.01 wt%), there must be ~16 wt% of VLT basalts. However, the relative abundances of REEs do not fit. Also, for this relatively high calculated VLT component it seems unlikely that we found only a few basaltic clasts comprising less than a few percent of the modal composition of DG. Even if the fragments of Fe-rich pyroxene came from basaltic rocks, the modal percentage of basalts would be not more than several percent. Further study is required to find other igneous components in DG matrix.

The high abundances of Ir (2.7 ppb for LG, 5.7 ppb for DG, and 9.3 ppb for IM) can be explained by meteoritic contamination. Warren and Wasson (1977) suggest that siderophile contents $<3 \times 10^{-4}$ times those of CI chondrites (~0.12 ppb) provide the most reliable evidence for pristinity. However, the Ir contents of LG, DG, and IM are significantly higher, consistent with textural evidence for multiple impacts.

In spite of petrographic evidence of impact mixing, the Y-86032 subsamples have very low Th (0.0765-0.191 ppm) and U (0.0258-0.056 ppm) abundances, confirming the absence of KREEP components (Fig. 4). Coupled with the low FeO contents, these data imply that a majority of the lithic components in Y-86032 originated from the far-side of the Moon. The variety of clast types reflects igneous, impact, and metamorphic processes occurring on the lunar highland crust. But, in spite of evidence of multiple impact and mixing, including fragments of more evolved rocks and possibly mare basalts, the extremely low Th and Fe contents in the Y-86032 breccia indicate that mixing was mostly limited to components from the lunar highland crust. In particular, the LG lithology contains a restricted suite of rocks that may be a mixture of similar and apparently related compositions that have not been found in previous studies, either of the Apollo samples, or of other lunar meteorites. The Sm-Nd age of 4.43±0.03 Ga from mineral separates from the DG and LG lithologies discussed below suggests that most of the rocks of the protolithic suite were cogenetic, and that the old age was preserved because the Sm-Nd system is difficult to reset by shock heating at the above temperatures.

4. Sm ISOTOPIC COMPOSITION OF Y-86032 LITHOLOGIES

Figure 5 summarizes the samples allocated for isotopic studies. The Sm isotopic compositions were measured for allocations from all Y-86032 lithologies and show only small variations from that of the terrestrial isotopic standard due to capture of thermalized neutrons (Table 1). For analytical reasons, the data are reported relative to two differenct normalizations. Older data for ,116 GC are reported normalized to our customary choice of $^{147}Sm/^{152}Sm = 0.56081$ (Wasserburg et al., 1981). However, because of neutron capture on ^{151}Eu , this is not a good choice for lunar highland samples with large Eu/Sm ratios; i.e., large positive Eu anomalies. This was not a significant problem for the earlier analysis of ,116GC because the secondary neutron fluence experienced by this sample was so low as to have an insignificant effect on the Sm-isotopic composition in any case. However, this is not the case for some of the other Y-86032 lithologies, dictating that ^{152}Sm not be used for normalization. Additionally, for this sequence of analyses we observed an unidentified interference at mass-147, making ^{147}Sm inappropriate for normalization. This effect was most noticeable for the ,37 IM sample for which the mass-147 interference was nearly 5 ε-units (parts in 10^4). Consequently, the Sm-isotopic data are most reliably normalized to $^{148}Sm/^{154}Sm = 0.49419$ (Wasserburg et al., 1981). Unfortunately, it was not possible to renormalize the older ,116GC analysis to $^{148}Sm/^{154}Sm$ because of interference by $^{138}Ba^{16}O$ as shown by the large uncertainty in the $^{154}Sm/^{152}Sm$ for that analysis. ^{147}Sm and ^{152}Sm are free of isobaric interference by other REE, which is our reason for preferring this ratio in most instances. Thus, we attribute the puzzling interference at mass-147 to unidentified molecular ions. There is a hint in the data for the other Y-86032 samples that this interference may have been generally present, only at much lower levels than for ,37 IM. We have not assigned formal error limits to the ,37 IM data on the assumption that smaller interferences may have been present at other masses as well. In any case, the key information is contained in the ^{149}Sm and ^{150}Sm abundances, which are displayed as ε-unit deviations from the terrestrial values in Fig. 6. In this representation, all of the data lie within analytical uncertainty of the n-capture line for conversion of ^{149}Sm to ^{150}Sm.

For ,28 LG as well as for the previously analysed ,116 GC, the decrease in ^{149}Sm abundance due to capture of thermalized neutrons is <~ 1 ε-unit (Fig. 6). Thus, the total neutron fluence experienced by these two lithologies was ~ 1 x 10^{15} n/cm^2. Significantly, the fluence experienced by any other lithology was only about twice as great. All the ε-values are about 100-fold less than for lunar highland meteorites MAC88105 and QUE93069, for example. They also are signficantly less than for most Apollo returned samples. Of the 14 mare basalts for which Nyquist et al. (1995) reported Sm-isotopic data, for example, only three of them have neutron-capture induced ^{149}Sm anomalies of <~-1 ε-unit: 70135, 74255, and lunar meteorite Asuka-881757. Of these, ε^{149}Sm = -1.2±0.4 for basalt 70135 is the closest match to the Y-86032 data. Arvidson et al. (1976) report a ^{81}Kr-Kr exposure age of 106±4 Ma for 70135 and suggested that the age possibly correlated with an influx of crater debris from the crater Tycho to the Apollo 17 site. The much younger noble gas exposure ages of 3-8 Ma for the Y-86032 samples discussed later suggest that most of their exposure to thermal neutrons occurred at deeper depths more completely shielded from the primary cosmic ray flux than was 70135.

The Sm-isotopic data for the Y-86032 samples are so similar that it is difficult to identify detectable differences in the neutron exposures of the various lithologies. There is a hint that the IM samples experienced somewhat greater neutron fluences than the other lithologies, qualitatively consistent with a longer regolith residence time as implied by the higher Ir contents of the impact melt sample. We note here that our allocation of ,30 consisted of an intimate mixture of IM and LG lithologies (*cf.* Fig. 1), and that the Sm-isotopic data were obtained on dominantly IM lithology, whereas the ^{39}Ar-^{40}Ar data reported below was for a sample of dominantly LG lithology. The Sm isotopic data are consistent with a relatively simple scenario in which little-exposed LG lithology was engulfed during initial brecciation by DG regolith material having slightly greater exposure to thermal neutrons and meteoritic contamination. Introduction of impact melt during final brecciation, as suggested by the textural observation, could have occurred soon thereafter, which would also be consistent with the close compositional similarity between the IM and DG material. By comparison to the 70135 data, the near-surface regolith exposure probably

occurred on a time scale short compared to 100 Ma. The ^{39}Ar-^{40}Ar data presented below show these events to have occurred early in lunar history. Thereafter, Y-86032 must have resided at a location largely shielded from thermalized neutrons; i.e., deep in the megaregolith. That Y-86032 was rather deeply buried in the megaregolith for most of its history prior to impact ejection from the lunar surface also is consistent with the low concentrations of solar wind Ar to be discussed later, and the near-absence of grain-surface-correlated Pb in leaches of sample ,118, (Tatsumoto and Premo, 1991). Those U-Pb analyses of ,118 also show that the primary igneous lithologies in Y-86032 came from low-^{238}U/^{204}Pb sources similar to that of Apollo 16 FAN 60025. This observation is consistent with the FAN-like chemical compositions of the LG and W lithologies. As already noted, capture of thermalized neutrons by ^{149}Sm occurs at greater subsurface depths than production of cosmogenic $^{38}Ar_{cos}$ discussed later in the paper. Thus, during that time when Y-86032 was shielded from secondary neutrons, it also would have been shielded from primary cosmic ray production of $^{38}Ar_{cos}$. Most of the cosmogenic $^{38}Ar_{cos}$ present in the meteorite must have been produced over relatively short time intervals when Y-86032 or its precursor materials were resident near the lunar surface.

5. CHRONOLOGY OF Y-86032

5.1 Sm-Nd Age

5.1.1 Relation of mineral separates to mineralogy **(Small type)**

Because the chronological studies do not utilize *in situ* techniques, a precise correlation of the isotopic data to sample mineralogy is not possible. Nevertheless, because of the absence of KREEP or other trace element rich components in the protolith(s) of the Y-86032 clast lithologies, and because of the low trace element abundances in olivine, the primary contributors to the isotopic data must be plagioclase and pyroxene in the protolithic rock suite. For the Sm-Nd and Rb-Sr isotopic studies, these two minerals were separated from bulk clastic material according to their differing densities.

Fig. 7 shows the separation procedures for the ,28 LG clast; procedures used for ,44 DG material were similar. In each case, the starting material for the separation procedures was ground to a grainsize

<75 μm. The grainsize of mineral clasts in LG are variable in the range ~30-250 microns. Thus, the grainsize used for mineral separation was comparable to or less than the size of typical mineral clasts in ,28 LG. A first separation was made at a density of 2.85 g/cm^3. The lighter fraction was dominantly plagioclase, part of which was saved, and part analysed. The denser fraction was separated again at 3.32 g/cm^3, to obtain samples labeled Px1 and Px2, respectively. The denser separate was the purest pyroxene, and for ,28, comprised only ~3% of the starting material by weight. These mineral separate yields can be compared to the modal abundances of anorthite (94.5%) with minor amounts (~5%) of pyroxene, olivine, silica minerals, and chromite. Of the minerals in the mode, anorthite and silica would go into the lighter (<2.85 g/cm^3) fractions, whereas pyroxene, olivine and chromite would go into the fraction >3.32 g/cm^3; i.e., the fraction labeled Px2. The "Px1" fraction of intermediate density (2.85-3.32 g/cm^3) likely contains some anorthite as well as mafic minerals because the combined weight (Px1+Px2) is 9.5 % of the total, which exceeds the petrographically observed modal abundance of mafic minerals in ,28. Although there may be some variation in the modal abundance of mafic minerals, this discrepancy is not critical to interpretation of the isotopic data. Fig. 8 shows that the heavier Px2 samples from both the LG-lithology ,28 and the DG-lithology ,44 were distinctly enriched in Sm and Nd abundances compared to bulk samples, displaying the characteristic HREE enrichment and LREE depletion of pyroxene. Because the Px2 samples have the largest Sm/Nd ratio, they are the ones that most determine the Sm-Nd age.

5.1.2 Sm-Nd Isotopic Data

Figure 9 shows that the Sm-Nd isotopic data (Table 2) yield a precise isochron age T = 4.43±0.03 Ga for combined data from LG ,28 and DG ,44. We have combined the data because these lithologies are not distinct isotopically. The isochron is primarily for ,28, being anchored by the ,28 whole rock data at the lowest $^{147}Sm/^{144}Nd$ ratio, and by ,28 Px2 at the highest $^{147}Sm/^{144}Nd$ ratio. The data for ,44 are completely consistent with the isochron. We attribute the coincidence of the data for ,28 whole rock and the ,44 plagioclase separate to the fact that the bulk composition of the LG-lithology is very anorthositic as shown by its low Fe content, the lowest among the LG, DG, and IM lithologies. The somewhat higher

$^{147}Sm/^{144}Nd$ ratio of bulk ,44 shows that this sample contained a greater abundance of mafic minerals. Pyroxene analyses show two pyroxene populations at relatively low and relatively high Fe abundances, respectively, suggesting that two different anorthositic rock types contributed to the protolith of the LG-lithology. If so, the more magnesian of these rock types would be more highly represented in the lighter Px1 separate, and the more ferroan in the heavier Px2 separate. Because all of the pyroxene separates lie on the isochron within rather small error limits of ~0.3 ε-units, the limit of precision for our mass spectrometric measurements, the Nd isotopic data suggest the two rock types were cogenetic. In particular, if one of these rock types crystallized from the LMO, it is likely that the other did, also, but perhaps at a slightly different stage in the crystallization sequence.

5.2 Rb-Sr Isotopic Data

Rb-Sr data for Y-86032 (Table 3) show that those phases that are dominated by plagioclase, including in particular the ,28 and ,44 plagioclase separates, as well as ,28 whole rock, are consistent with the Rb-Sr systematics of Apollo 16 ferroan anorthosites like 60025 (Fig. 10). Plagioclases from several other Apollo 16 FAN samples also form an apparently isochronous relationship with the 60025 and Y-86032 plagioclases, which have the lowest Rb/Sr ratios. An isochron fitted to the Apollo 16 FAN plagioclase data gives an apparent age of 4.62±0.89 Ga and initial $^{87}Sr/^{86}Sr$ = 0.699066±43, where the 2σ uncertainty refers to the last digits. Although the isochron age is too imprecise to give a useful independent estimate of the time of original crystallization of these plagioclases, it nevertheless is consistent with the ~4.4 Ga Sm-Nd ages of 60025 and Y-86032, and the Ar-Ar age of Y-86032,116 presented below. Among the Y-86032 subsamples, 28 Px2, 44 Px2, 44 Px1, and the impact melt samples fall off the isochron. These subsamples were open Rb-Sr systems in the interval after ~4.4 Ga. The subsamples that plot above the isochron show the effect of Rb loss and/or Sr gain during one or more secondary events, and it is impossible to derive any chronological information from them. We attribute this either to weathering in the Antarctic environment, or possibly to enhanced processing blanks for these mg-sized samples (Table 3). Thus, we give no time significance to those data. The analysis of the 21-mg

sample ,33 IM, however, is robust, and its displacement from the alignment of the other robust analyses is significant. No mixing end member that could explain the high Rb/Sr ratio of the impact melt has been identified. We tentatively attribute the higher Rb/Sr ratio of ,33 IM to partitioning of Rb into the melt during impact melting. In this case, the tie-line between it and ,28 Plag giving an apparent age of 4.00±0.17 Ga is a probable upper bound to the time of the melting event. This "age" is within the likely range of ages derivable below from the Ar-Ar data for this lithology.

5.3 Ar-Ar Ages of Distinct Y-86032 Lithologies

5.3.1 Experimental **(Small type)**

Four different samples of Y-86032, along with several samples of the NL-25 hornblende age monitor, were irradiated with fast neutrons at the University of Missouri Research Reactor (MURR). The irradiation constant, J, for,116GC was 0.0312 ±0.003. This irradiation used BN to shield thermal neutrons. The irradiation constants for a separate irradiation of samples ,28 (LG-lithology) and ,33 (IM-lithology) were 0.0214 ±0.0001 and 0.0215 ±0.0015, respectively. A third irradiation of sample ,30 (DG-lithology) gave a J value of 0.02051 ±0.00003. Each sample was degassed by stepwise heating in a furnace equipped with a thermocouple, and the argon isotopes were measured on a VG-3600 mass spectrometer. Uncertainties reported for individual ages include errors in measuring the $^{39}Ar/^{40}Ar$ ratio and uncertainties in blank and reactor corrections. Because reactor corrections are large for samples with high Ca/K ratios, we went to considerable effort to define these corrections precisely for our MURR irradiations. This included determining more precisely the half-life of ^{37}Ar, which is the measured parameter used to make such corrections, and documenting effects of fuel cycle on correction factors. These data are presented and discussed in Appendix 1. Other experimental details are given in Bogard et al. (2000).

5.3.2 Y-86032,116.

The Ar-Ar age spectrum for a 17.1 mg subsample of Y-86032,116GC is presented in Fig. 11. Reactor corrections to ^{39}Ar for most extractions were ~40%. The measured [K] of 74 ppm and [Ca] of

12.2% are consistent with nearly pure anorthite. The K/Ca ratio is constant at ~6 x 10^{-4} throughout the release, and most of the Ar was released at relatively high temperatures of 1100-1400°C. The first four extractions (0-15% ^{39}Ar release) show decreasing ^{36}Ar/^{37}Ar and ^{36}Ar/^{38}Ar ratios and Ar-Ar ages, consistent with release of adsorbed terrestrial Ar. Intermediate temperature extractions show increasing Ar-Ar ages indicative of prior ^{40}Ar diffusion loss. No age plateau is attained. However, the 1400°C extraction released 28% of the total ^{39}Ar and gives an age of 4.414 ±0.035 Gyr (where the error includes the uncertainty in irradiation constant, J). Because of the possibility of ^{40}Ar diffusion loss from even the 1400°C extraction, this is a lower limit to the Ar retention age.

We must consider corrections to this age necessitated by ^{40}Ar implanted from the lunar atmosphere along with solar wind ^{36}Ar and ^{38}Ar. For eight extractions (releasing 15.5-99.5% of the ^{39}Ar), the measured ^{38}Ar/^{36}Ar ratios vary a factor of two and the ^{37}Ar/^{36}Ar ratios vary a factor of three. This variability indicates a mixture of two components – trapped solar wind Ar and a nuclear component consisting of ^{38}Ar and ^{36}Ar produced from Ca by cosmic rays plus ^{37}Ar produced from Ca in the reactor. A plot (not shown) of ^{38}Ar/^{37}Ar versus ^{36}Ar/^{37}Ar for these eight extractions is linear (R^2=0.9935), which indicates the solar and nuclear components have essentially constant Ar isotopic compositions. This plot gives a trapped ^{38}Ar/^{36}Ar of 0.1925 ±0.0064 and a slope of 0.00152 ±0.00002. Adopting cosmogenic ^{36}Ar/^{38}Ar=0.67, this slope indicates a constant nuclear ^{37}Ar/^{36}Ar component of 661±8 across these eight extractions. From the nuclear ^{37}Ar/^{36}Ar ratio, we calculated the cosmogenic ^{36}Ar for each extraction. Cosmogenic ^{36}Ar comprised 35% of the total ^{36}Ar released at 1400°C, for example. The solar wind ^{36}Ar concentration for each extraction was then determined by subtracting $^{36}Ar_{cos}$ from the measured ^{36}Ar (see Garrison et al. (2000) for details).

Studies of many Apollo samples have shown that solar wind ^{36}Ar is always accompanied by an implanted ^{40}Ar component, where the ^{40}Ar/^{36}Ar ratio is typically ~0.3-1.0 for material exposed at the lunar surface within the past ~1 Gyr. However, lunar samples exposed to the solar wind much earlier are believed to contain significantly higher trapped ^{40}Ar/^{36}Ar ratios, and samples exposed as early as ~4 Gyr

ago may contain ratios of ~10 (McKay et al. (1986), Fig. 6). We do not know the trapped $^{40}Ar/^{36}Ar$ ratio in Y-86032,116, but we can assume various ratios and apply corrections to measured ^{40}Ar. Applying such a ^{40}Ar correction by assuming trapped $^{40}Ar/^{36}Ar$ = 2, 5, and 10 gives corrected ages for the 1400°C extraction of 4.408 ±0.035, 4.397 ±0.035, and 4.380 ±0.035 Gyr, respectively. Thus, the Ar-Ar age of the 1400°C extraction of Y-86032,116 likely lies in the range 4.38-4.41 ±0.035 Gyr. Because the 1400°C extraction also may have lost some of its ^{40}Ar by diffusion, it is possible that the original Ar-Ar age of this clast is identical to the 4.43 ±0.04 Gyr Sm-Nd isochron age presented above for Y-86032 lithologies.

5.3.3 Y-86032,28.

The Ar-Ar age spectrum for a 27.3 mg subsample of the LG-lithology is presented in Fig. 12. Reactor corrections to ^{39}Ar for most extractions were ~25%. The measured [K] and [Ca] are 145 ppm and 11.0%, respectively. The K/Ca ratio of the Ar-Ar sample was relatively constant at ~0.002 and most of the Ar was released at temperatures of 1150-1400°C. Higher K/Ca ratios in the first two extractions suggest addition of K to grain surfaces, possibly during Antarctic weathering. The first few extractions (~0-10% ^{39}Ar release) show decreasing $^{36}Ar/^{37}Ar$, $^{36}Ar/^{38}Ar$, K/Ca ratios, and Ar-Ar ages, consistent with release of adsorbed terrestrial Ar. A steady increase in age across 17-39% ^{39}Ar release suggests some ^{40}Ar diffusion loss. However, eight extractions releasing ~39-100% of the ^{39}Ar show an age plateau with an average value of 4.108 ±0.017 Gyr (including the uncertainty in J).

There is only minimal evidence for trapped solar wind ^{36}Ar in sample LG,28. The absence or near-absence of solar wind Ar in this sample is consistent with the short regolith-residence time indicated by the the low thermal neutron fluence in this sample (Fig. 6). Above ~8% ^{39}Ar release the measured $^{36}Ar/^{38}Ar$ ratio is relatively constant at approximately the expected cosmogenic value. An exception is the 1220°C extraction, where increases in both the $^{36}Ar/^{38}Ar$ and $^{36}Ar/^{37}Ar$ ratios suggest release of trapped ^{36}Ar. Among those eight extractions that define the age plateau, we adopted the highest measured $^{37}Ar/^{36}Ar$ ratio to represent a pure nuclear component and applied corrections for trapped ^{36}Ar to the remaining extractions (see above). Assuming trapped $^{40}Ar/^{36}Ar$ ratios of 5 and 10, the corrected plateau

ages are 4.104 ±0.017 and 4.099 ±0.017 Gyr, respectively. Thus, we adopt an age of 4.10 ±0.02 Gyr for Y-86032,28. The age spectrum in Fig. 12 shows the age corrected for trapped $^{40}Ar/^{36}Ar = 5$.

5.3.4 Y-86032,33.

The Ar-Ar age spectrum for a 29.5 mg subsample of IM impact melt is presented in Fig. 13. The measured [K] and [Ca] are 210 ppm and 11.8%, respectively, and the K/Ca ratio is relatively constant at ~0.0017 across most of the ^{39}Ar release. Most of the ^{39}Ar is released at relatively high temperatures of 1150-1400^{o}C, suggesting that the K is hosted in retentive phases. The first seven extractions (0-9% ^{39}Ar release) show significantly decreasing K/Ca and $^{36}Ar/^{37}Ar$ ratios and Ar-Ar ages, which are indicative of weathering effects. Over ~20-100% ^{39}Ar release the Ar-Ar age shows apparently random scatter considerably in excess of individual analytical uncertainties. In this range, the maximum and minimum ages (uncorrected for trapped ^{40}Ar; see below) are 4.37 and 4.17 Gyr. Over 20-100% ^{39}Ar release, the $^{36}Ar/^{38}Ar$ ratio is relatively constant at 2.62 ±0.08 and indicates the presence of significant amounts of solar wind ^{36}Ar. As discussed above, we do not know the trapped $^{40}Ar/^{36}Ar$ ratio within Y-86032, but it may be as high as ~10. Thus, in Fig. 13 we show the ages both without any trapped ^{40}Ar correction and with a correction assuming $^{40}Ar/^{36}Ar = 10$. This ^{40}Ar correction lowers these maximum and minimum ages to 4.06 and 3.87 Gyr. Corrections assuming trapped $^{40}Ar/^{36}Ar$ ratios between 0 and 10 would give intermediate ages. However, even with this maximum correction for lunar atmospheric ^{40}Ar, the individual ages still display significant scatter, which is larger than the uncertainties in individual ages. A plot of $^{40}Ar/^{37}Ar$ versus $^{36}Ar/^{37}Ar$ also shows significant scatter, confirming that the ^{40}Ar is not proportional to the nuclear component. We suggest that this scatter in individual Ar-Ar ages is produced by the melt having incorporated materials of old and possibly differing ages, which were not totally degassed of their radiogenic ^{40}Ar at the time of melt injection. The absolute earliest time of formation of the melt would be ~4.17 Gyr, as given by the uncorrected age, and ~4.10 Gyr, which is the age of the ,28 clast, corrected for implanted ^{40}Ar. A considerably lower maximum age for melt formation would be obtained if we correct for lunar atmospheric ^{40}Ar using trapped $^{40}Ar/^{36}Ar = 10$, and with such a ^{40}Ar

correction the formation age for the melt could be as young as ~3.9 Gyr. The age of the melt could be even younger if considerable undegassed radiogenic ^{40}Ar was released in those extractions giving the youngest Ar ages.

Interestingly, the [Ca] content of this impact melt (11.8%) is nearly as high as that for ,116 GC (12.2%), suggesting that the protolith for the impact melt was dominantly anorthositic. The origin of the two-fold higher [K] content is not currently discernible, but is unlikely to be a KREEP component. Note in Fig. 3 that the Heavy Rare Earth Elements (HREE) in the DG and IM-lithologies are relatively more enriched than the Light Rare Earth Elements (LREE), whereas KREEP is LREE-enriched. Thus, the source of REE in IM and DG relative to LG is probably a mafic component as already discussed. As with the other small subsamples analysed for Ar-Ar, sample heterogeneity plays a role. Thus, larger samples of impact melt analysed by INAA at Tokyo Metropolitain University (Karouji et al., 2004) had slightly lower average [Ca] = 11.0% and variable [K] from 107 to 367 ppm. The average [K] = 237 ppm is similar to [K] = 210 ppm for the Ar-Ar subsample. At the lower end of the [K] range, [K] = 107 ppm suggests that melts of very anorthositic composition remain incompletely homogenized within the IM-lithology at the scale of the samples used for INAA analysis.

5.3.5 Y-86032,30.

The Ar-Ar age spectrum (Fig. 14) for this sample of the DG lithology located adjacent to the impact melt is very similar to that for sample ,33 IM. Our allocation of this lithology contained both light (~LG and/or ~W) and dark (~IM) material (Fig. 1). Note that the sample used for Ar-Ar was enriched in light material, whereas that used for Sm-isotopic measurements was enriched in impact melt. The first five extractions (0-11% of the ^{39}Ar) released adsorbed terrestrial Ar, and an isochron plot of these data (R^2=0.995) give an ^{40}Ar/^{36}Ar intercept close to the terrestrial value and an age of ~0.97 Gyr. We ascribe no time significance to this “age”, because it is associated with weathered phases. All extractions up to ~30% of the ^{39}Ar release indicate prior diffusion loss of radiogenic ^{40}Ar. Above ~40% ^{39}Ar release the uncorrected Ar-Ar ages tend to vary over ~4.16-4.35 Gyr, a similar age range to that shown by sample ,33.

Like sample ,33, sample ,30 also released significant quantities of trapped solar wind ^{36}Ar with a nearly constant $^{36}Ar/^{38}Ar$ ratio of ~2.5. Thus, a correction to the Ar ages is probably required for lunar atmosphere ^{40}Ar. Fig. 14 shows the Ar-Ar ages assuming trapped $^{40}Ar/^{36}Ar$ ratios of 0 and 10. As with IM ,33, the maximum ^{40}Ar correction produces ages (for >45% ^{39}Ar release) of 3.94-4.03 Gyr, values similar to the corrected ages of IM ,33. Thus the Ar ages of samples IM ,33 and DG, 30 are quite similar.

6. DISCUSSION

6.1 Chronology and the Age of the Protolith

The Sm-Nd age of 4.43±0.03 Ga indicates early formation of the protolith of Y-86032. The lower limit of 4.35-4.41 Gyr for the Ar-Ar age of ,116GC may still be influenced by ^{40}Ar diffusive loss and the Ar-Ar age may be consistent with the Sm-Nd age. As discussed earlier in the paper, although remnants of different rock types are present in the breccia, the protolith was dominantly feldspathic. Although the modal mineral abundances in LG resemble those in FANs, the detailed mineral chemistry differs from that of FANs (Yamaguchi et al., 2004, 2005). Nevertheless, REE abundances in the W and LG litholgies are only slightly enriched relative to those in FANs (Karouji et al., 2004). Thus, it is reasonable to compare the Sm-Nd data for the Y-86032 samples to those of FANs from other lunar localities, especially from the Apollo 16 site. The Sm-Nd age of the combined LG and DG lithologies and the Ar-Ar age of W,116 are similar to the crystallization age of ferroan anorthosite 60025 (Carlson and Lugmair, 1988). Because the analysed samples were breccias, both the Ar-Ar and Sm-Nd ages are lower limits to the age of the protolith; i.e., to the age(s) of the suite of rocks contributing to the breccias. Thus, three types of data, the Ar-Ar age of Y-86032 ,116GC, the Sm-Nd age of the combined LG- and DG-lithologies Y-86032,28 and Y-86032,44, and the Sm-Nd age of FAN 60025 indicate formation of the lunar crust by ~4.4 Ga ago.

The younger Ar-Ar age of 4.10 ±0.02 Gyr for LG ,28 indicates thorough Ar outgassing prior to lithification of the breccia. The Sm-Nd age is much more difficult to reset, since that would require Nd-isotopic equilibration between plagioclase and pyroxene. As shown by the Ar-Ar study, complete Ar loss

from the protolith of Y-86032 was not achieved even during formation of the impact melt lithology. REE diffusion is much more difficult than Ar diffusion, and is particularly sluggish in pyroxene. Thus, preservation of the Sm-Nd age of ,28 in spite of resetting of its Ar-Ar age is not unreasonable.

When did the Y-86032 breccia form? As shown by the above considerations, the age of the melt is not well constrained. The Ar-Ar ages of clasts ,116GC and ,28LG probably were set by impact heating events prior to breccia formation. The very flat plateau age of ,28 suggests that lithic components contributing to it were totally degassed of Ar during formation of the LG lithology. The final assembly of the breccia was coincident with injection of the impact melt. The Ar-Ar data on LG and impact melt samples suggest a formation time ~3.9 Gyr ago. A Rb-Sr tie line age for the impact melt gives an age of 4.00±0.17 Ga consistent with the range of ages shown in Fig. 13 and 14, and suggesting that the impact melt was not formed significantly later than 3.9 Ga ago. It appears that the breccia was assembled during the time period of the hypothesized "lunar cataclysm" ~3.9 Ga ago. In any case, it also is clear that Y-86032 contains breccia components lithified prior to the time period customarily ascribed to the lunar cataclysm, at least as early as ~4.1 Ga ago, and possibly as early as ~4.38 Ga ago.

6.2 Cosmic Ray Exposure Age

We analyzed a 33 mg unirradiated sample of Y-86032,116GC, for cosmogenic He, Ne and Ar in order to estimate its exposure time to cosmic rays. In addition to cosmogenic gases, significant amounts of trapped Ne and Ar were also present. We assumed this trapped component to have the composition of solar wind implanted into typical lunar surface material and calculated abundances of cosmogenic ^{21}Ne and ^{38}Ar. These were 99% and 32%, respectively, of the measured isotopic abundances. Cosmogenic concentrations were (in units of 10^{-8} cm^{3}STP/g): ^{3}He=5.4, ^{21}Ne=0.53, and ^{38}Ar=2.2. We can also estimate the concentration of $^{38}Ar_{cos}$ from each irradiated sample by assuming Ar is a mixture of cosmogenic and trapped components and by omitting apparent terrestrial Ar released at low temperatures. In the case of sample LG,28 essentially all of the ^{38}Ar is cosmogenic. The concentration of ^{38}Ar in irradiated samples ,116 GC and LG ,28 are each ~2.2 x10^{-8} cm^{3}STP/g, identical to $^{38}Ar_{cos}$ in the unirradiated sample

of ,116 GC. Calculated $^{38}Ar_{cos}$ concentratrions in IM ,33 and DG ,30 are higher at 5.0 and 3.4 $x10^{-8}$ cm^3STP/g, respectively. Because of larger relative concentrations of solar Ar in these two samples, their $^{38}Ar_{cos}$ concentrations should be considered more uncertain. However, it is also reasonable to expect that the surface-irradiated material that contributed solar wind Ar to these samples also contained larger amounts of $^{38}Ar_{cos}$.

To estimate cosmic ray exposure ages, we assumed the chemical composition to be that of pure anorthite and used the element-based production rates given by Eugster and Michel (1995) to calculate production rates for these nuclides. Because $^{38}Ar_{cos}$ production from Ca greatly dominates over that from Fe in all samples, the presence of even a few percent Fe would change the ^{38}Ar production rate very little. These production rates assume 4-π irradiation in space. Irradiation on the lunar surface would give rates lower by approximately a factor of two, and proportionately higher cosmic ray exposure (CRE) ages. Calculated CRE ages for ,116GC are ^{3}He=3.1 Myr, ^{21}Ne=2.7 Myr, and ^{38}Ar=8.5 Myr. It is not clear why the Ar age is three times the He and Ne ages. However, comparable amounts of ^{3}He and ^{21}Ne were released in the 400^{o}C extraction as in the 1600^{o}C extraction, whereas only ~3% of the ^{38}Ar was released at 400^{o}C. Feldspar is known to readily lose cosmogenic He and Ne, and part of the cosmogenic He and Ne in Y-86032 may have been lost. Because the Ar-Ar ages indicate samples ,116GC and LG ,28 had different histories prior to breccia assembly, identical $^{38}Ar_{cos}$ concentrations for these two samples suggest that their cosmic ray exposure mainly occurred after breccia assembly.

6.3 Initial ε_{Nd} of the protolithic lunar crust and the LMO

Figure 15 shows that, in contrast to some of the Apollo 16 anorthosites, the initial ε_{Nd} value from the combined data for Y-86032,28 and Y-86032,44 are consistent with formation of the protolithic lunar crust via plagioclase flotation from a Lunar Magma Ocean (LMO) of initially chondritic relative REE abundances. If the LREE enrichment that is characteristic of lunar FANs was produced early in lunar history from an LMO of initially chondritic relative REE abundances, one would expect a zero or possibly negative ε_{Nd} value. This is because, by definition, ε_{Nd} is the deviation of initial $^{143}Nd/^{144}Nd$

measured for a sample from the value that would exist in a reservoir of the same age that always had been characterized by chondritic relative REE abundances. By convention, one usually calculates $\varepsilon_{Nd\ CHUR}$ relative to an interlaboratory-adjusted initial $^{143}Nd/^{144}Nd$ value for a **Ch**ondritic **U**niform **R**eservoir, the parameters of which have been given by Jacobsen and Wasserburg (1984). For the isochron for the combined ,28 and ,44 data, $\varepsilon_{Nd\ CHUR}$ is +0.19±0.13. However, ε_{Nd} for these data is more appropriately calculated as $\varepsilon_{Nd\ HED}$ = -0.64±0.13 relative to initial $^{143}Nd/^{144}Nd$ obtained in the JSC lab for HED meteorites (Nyquist et al., 2004). The difference between the two values is shown in Fig. 15, where all ε_{Nd} values are shown relative to $\varepsilon_{Nd\ HED}$ = 0.

Fig. 15 compares ε_{Nd} values for Y-86032 subsamples to literature data for Apollo 16 FANs and KREEP-rich samples. As noted, the slightly negative value of ε_{Nd} at 4.43 Ga ago from the isochron of Fig. 9 is consistent with derivation of the protolithic lithologies from the LMO following crystallization of mafic mantle cumulates. The earlier data for ,116GC plotted at the Ar-Ar age suggest that the anorthositic lunar crust may have been even more LREE-enriched than lunar KREEP. However, similar data would have to be obtained by internal isochron techniques before this conclusion could be considered to be robust. Importantly, the Y-86032 Nd-isotopic data do not imply derivation of lunar anorthosites from an earlier LREE-depleted reservoir, as do many of the data for Apollo 16 FANs. The reason why the Apollo 16 data show this feature is not well understood. The most likely possibility seems to be partial Nd-isotopic equilibration related to significant exogenic thermal inputs into the lunar crust from major basin-forming impacts on the lunar nearside. However, the possibility of "late" generation of some anorthositic highland lithologies that are not directly connected to the LMO; i.e., serial magmatism (Walker et al., 1983), should not be dismissed completely.

Fig. 15 also shows ε_{Nd} for ,33 IM calculated at the Rb-Sr tie-line age of 4.00±0.17 Ga (Fig. 9). The datum calculated plots close to the evolution line corresponding to $^{147}Sm/^{144}Nd$ ~0.17 in KREEP source regions. The low Th abundance in Y-86032 excludes the presence of significant KREEP in the impact melt, but 'Mg-suite' norites and troctolites also have source regions with $^{147}Sm/^{144}Nd$ ~0.17 (Shih

et al., 1993). Thus, mixing end-members for the IM melt, in addition to components present in the LG breccia, are most likely to be found among rocks that, like KREEP and the Mg-suite, contain an urKREEP component. The negative value of ε_{Nd} for ,33 IM provides a constraint on the type and amount of mare basalt components that might have been incorporated into the melt when it solidfied. For example, the ~3.9 Ga age of the Asuka 881757 lunar meteorite (Misawa et al., 1993) suggests material like it could have been mixed into the Y-86032 impact melts, but the large, positive ε_{Nd} ~7 for A-881757 makes this seem unlikely. Nevertheless, quantitative modeling with a large range of possible end-member components has not yet been done.

6.4 Initial $^{87}Sr/^{86}Sr$ of the protolithic lunar crust

Determining constraints for the chronological and geochemical evolution of the LMO and the later evolution of the bulk moon has been a long-standing goal of lunar isotopic studies. The new initial Sr isotopic data of Y-86032, combined with data for FANs and "benchmark" values of initial $^{87}Sr/^{86}Sr$ for more primitive objects provide one approach to this goal. Figure 16 compares $^{87}Sr/^{86}Sr$ for the Y-86032 lithologies and lunar FANs to data for plagioclase from basaltic eucrites and initial $^{87}Sr/^{86}Sr$ from Efremovka CAI E38 (Nyquist et al., 2004). Plagioclase ought to be particularly robust to post-crystallization thermal events that may have affected the eucrites as well as the lunar samples. It is apparent from Fig. 16 that the rocks of the lunar crust had higher $^{87}Sr/^{86}Sr$ ratios at ~4.4 Ga ago than did the eucrites. The latter are crustal rocks of the HEDPB (Howardite-Eucrite-Diogenite Parent Body), thought to be the asteroid 4 Vesta. This observation immediately prompts inquiry into the conditions leading to this result.

A first observation is that the initial $^{87}Sr/^{86}Sr$ ratios in the earliest crustal samples from both the moon and the HEDPB are evolved compared to initial $^{87}Sr/^{86}Sr$ in the E38 Calcium Aluminum Inclusion (CAI) from Efremovka. Since CAIs are thought to have formed in the solar nebula at the very beginning of solar system history, this observation suggests that part of the variation in initial $^{87}Sr/^{86}Sr$ among CAIs, Vesta, and the moon is due to evolution of $^{87}Sr/^{86}Sr$ in the solar nebula. A customary assumption is that

the non-volatile composition of the nebula was similar to that of CI chondrites, which have comparatively high $^{87}Rb/^{86}Sr$ ~0.91. Radiogenic growth of $^{87}Sr/^{86}Sr$ from ~0.698934 found in E38 with this $^{87}Rb/^{86}Sr$ ratio in the solar nebula would lead to $^{87}Sr/^{86}Sr$ ~0.699004 for Vesta and $^{87}Sr/^{86}Sr$ ~0.699056 for the moon in time intervals of only ~5 and 10 Ma, respectively. These are not unreasonable time periods given the differing sizes of Vesta and the moon. Additionally, for Vesta, this calculation suggests that the oldest eucrites should be ~(4567-5) = 4562 Ma old. Directly measured zircon ages of five eucrites average 4554±7 Ma (Misawa et al., 2005); i.e., are ~13 Ma younger than CAI, suggesting a slower rate of growth of $^{87}Sr/^{86}Sr$ corresponding to average $^{87}Rb/^{86}Sr$ ~ 0.38. A similar calculation for $^{87}Rb/^{86}Sr$ ~ 0.38-0.91 suggests that the age of lunar crustal rocks ought to be ~4557-4544 Ma, significantly older than the ages of the FANs determining our best estimate of the lunar initial $^{87}Sr/^{86}Sr$ ratio.

In the case of the moon, it is reasonable to assume that the difference between the age estimated from initial $^{87}Sr/^{86}Sr$ ratios and the actual age of lunar crustal rocks can be ascribed to a period of radiogenic growth at a much lower $^{87}Rb/^{86}Sr$ ratio than that in the solar nebula. Indeed, Nyquist et al. (2001) estimated a bulk moon $^{87}Rb/^{86}Sr$ ratio of 0.038. Using this Rb/Sr ratio, Nyquist and Shih (2005) examined various scenarios for lunar formation. It is reasonable to assume, for example, that proto-Earth had grown in the nebula for at least 5 Ma (equivalent to the growth time of the HEDPB) before being struck in the "Giant Impact" leading to the moon's formation. Volatile and moderately volatile elements like Rb would be lost to space in the impact. An estimate of the duration of the ensuing magma ocean period of lunar history can be derived from the difference between the eucrite and FAN initial $^{87}Sr/^{86}Sr$ ratios and the post-impact $^{87}Rb/^{86}Sr$ ratio of the bulk moon. An estimate of ~100 Ma for the duration of lunar crustal formation results for $^{87}Rb/^{86}Sr = 0.038$, in agreement with thermal models for lunar evolution, such as the one by Solomon and Longhi (1977). More complex scenarios presented orally by Nyquist and Shih (2005) are reserved for a later publication.

6.5 Early crustal bombardment history

Textural relationships show that the DG-lithology was formed by impact lithification of regolith composed of various highland igneous/metamorphic components, impact melt clasts, and minor contributions of mare basalts. The presence of impact melt clasts in DG suggests that some of these components had already experienced impact events before lithification. The LG-lithology is likely to have been a breccia of a single suite of igneous rocks prior to final breccia assembly because of the proximity of components within it. Whether the LG was a small fragment of an igneous rock, or from an older breccia generation is unclear. The range of mineral compositions observed in LG suggest that it was from an older generation breccia. Grain-boundary melting is likely to have occurred at this time because pore spaces (in the regolith) would have effectively raised temperatures to cause melting. The elongated shape and gradational (not well-defined) boundaries of LG suggests shear deformation during lithification, or by later impact events. A final impact event produced the IM-lithology cutting across both DG and LG. Thus, based on its texture, this breccia experienced more than two impact events. There also may have been impact and thermal events not recorded in its mineralogy and petrology.

The Sm-isotopic data are broadly but perhaps not totally consistent with the above interpretation of the textural relationships. The thermal neutron fluence experienced by the LG lithology is among the lowest measured for the Y-86032 lithologies for which the textural relationships are discernible in Fig. 1. However, several of the DG subsamples experienced similarly low neutron fluences, so it cannot be argued from the basis of the Sm data that the LG lithology existed separately from the DG lithology prior to final brecciation. Neither, however, can it be argued that it did not. The impact melt samples show the greatest neutron-capture effects, and also the highest concentration of Ir, indicating the greatest meteoritic contamination. Thus the neutron fluence and siderophile element data are consistent with injection of the impact melt as the last event in breccia assembly. The difference in neutron capture effects between IM and LG is so small that it cannot be clearly resolved. The higher Ir content of IM is consistent with its introduction at the last stage of breccia formation. The Sm isotopic data suggest the breccia was formed rather rapidly with no long intervening periods (on the order of 100 Ma) when the individual breccia components were separately resident in the lunar regolith.

The Ar-Ar data are qualitatively consistent with the textural relationships. The well-defined Ar-Ar age of 4.10±0.02 Ga and low trapped gas content of the LG-lithology is consistent with its existence as a single clast prior to an impact event which totally outgassed its Ar. The Ar-Ar age spectra of the IM and DG lithologies as recorded in subsamples ,33 and ,30, respectively, are consistent with later formation of the melt during breccia assembly if plausible corrections are made for the presence of trapped Ar. However, the presence of inherited, undegassed, radiogenic ^{40}Ar in the IM lithology prevents unambiguous determination of its formation age. The Rb-Sr tie-line age of 4.00±0.17 Ga suggests formation of the IM lithology close to the formation time of the 4.1 Ga LG lithology, and consistent with the Ar-Ar ages obtained for IM ,33 and DG ,30 assuming trapped ^{40}Ar/^{36}Ar = 10 (Fig. 13, 14). In this case, final breccia assembly may have occurred during the hypothesized ~3.9 Ga lunar cataclysm (Tera et al., 1974). The probable farside origin of Y-86032 thus allows extension of the cataclysm hypothesis to the lunar farside.

The presence of solar wind components in the IM-lithology suggests that these melts were formed by melting of regolith located near the surface, and injected into the precursor breccia. The precursor breccia itself apparently consisted of a regolith component (DG) and a more nearly pristine component (LG), thereby lithologically resembling a polymict eucrite. Nyquist et al. (1986) in their study of a pristine clast in polymict eucrite Y-75011 suggested that polymict eucrites likely were formed by impact excavation to the surface of the parent body, whereas monomict ordinary eucrites may have remained near crater floors or along crater walls following an impact event. This suggestion was founded on cratering studies that show monomict breccias are found on the floors and along the walls of impact craters (Kieffer and Simonds, 1980; Stöffler, 1981). Thus, such a geologic setting for the LG clast prior to its excavation and mixing with DG regolith may be likely. Although it is not possible to specify the geologic setting uniquely, it is significant that only a few major impacts were involved in forming the Y-86032 breccia. It is also significant that more than one major impact is required, and that the evidence of individual impacts has been retained, and not obliterated. The $^{38}Ar_{cos}$ and ^{149}Sm data indicate that the final,

assembled breccia was buried at a depth of at least a few meters probably from the time of breccia assembly ~3.9 Ga ago until launched on its way to Earth <~3-8 Ma ago.

7. CONCLUSIONS

The combined mineralogical, chemical, and chronological study of Y-86032 suggests formation of the farside lunar crust at or before 4.43±0.03 Ga ago. This conclusion is based on the Sm-Nd age of the combined LG and DG lithologies, and strongly supported by the Ar-Ar age of ,116GC. It also is less strongly supported by the maximum Ar-Ar ages of two impact melt samples from the breccia, both of which give maximum Ar-Ar ages for individual temperature steps of ~4.35-4.37 Ga. The close agreement of these maximum ages with the age of ,116GC, and also with the Sm-Nd age of combined LG and DG lithologies seems more than coincidental.

We interpret the fact that combined Nd-isotopic data from DG and LG lithologies lie on a single Sm-Nd isochron within error limits as meaning that the farside protolith from whence Y-86032 came contained a limited range of cogenetic FAN and FAN-related lithologies. Additionally, the initial $^{143}Nd/^{144}Nd$ present in the protolith when it solidified is consistent with crustal formation via plagioclase flotation on the LMO. The coincidence in initial $^{87}Sr/^{86}Sr$ for ancient crustal samples from the lunar nearside (Apollo 16 FANs) and lunar farside (Y-86032 lithologies) is consistent with the concept of a global LMO. Furthermore, the initial $^{87}Sr/^{86}Sr$ present in the protolith when it solidified is consistent with radiogenic growth of ^{87}Sr in the LMO at a rate corresponding to $^{87}Rb/^{86}Sr$ ~0.038 estimated for the bulk moon.

Some of the impact lithologies in Y-86032 were formed prior to the hypothesized cataclysmic bombardment of the lunar surface about 3.85-3.95 Ga ago, as shown most clearly by the 4.10±0.02 Ga Ar-Ar age of LG lithology ,28. The >4.35 Ga Ar-Ar age of ,116GC also may be related to impact processes, but more probably represents substantial retention of an original crystallization age similar to the ~4.43 Ga Sm-Nd age of the combined LG and DG lithologies. The present Ar data do not unambiguously determine the time of final breccia assembly because the trapped $^{40}Ar/^{36}Ar$ ratios in the impact melt are poorly constrained, and because there is strong evidence that phases in the impact melt

were not totally degassed during impact melting. Nevertheless, the Ar data indicate that probably the breccia assembly event was not earlier than ~3.9 Gyr ago. Considering the additional evidence provided by the Rb-Sr and Sm-Nd data for ,33 IM we favor final breccia assembly at ~3.9 Ga ago, within the time frame hypothesized for the lunar cataclysm.

The presence of clasts in Y-86032 with differing Ar-Ar ages implies multiple impact heating events. In particular, impacts occurring during an early period of bombardment from 4.1 – 4.35 Ga ago have been preserved. This observation poses the question of how these Ar-retention ages survived the hypothesized later cataclysmic bombardment (Tera et al., 1974), or if not a "cataclysm" then the "Late Heavy Bombardment" (*cf.* Hartmann, 2003). That Y-86032 spent a significant portion of its existence deeply buried in a megaregolith far distant from basin-forming impacts seems a likely explanation, and is consistent with the evidence from cosmogenic noble gases and thermal neutron capture effects.

Acknowledgements - This research was supported by a Grant-in-Aid for Scientific Research from the Ministry of Education, Science and Technology, Japan, No. 12740300 (AY) and by NIPR Research Project Funds, P-8 (Evolution of the early Solar System materials). Research at the Johnson Space Center was supported by NASA RTOP 344-31 to L. E. Nyquist and D. D. Bogard. We thank H. Kojima for discussion and the sample preparation of Y-86032.

REFERENCES

Arvidson R., Drozd R., Guiness E., Hohenberg C., Morgan C., Morrison R., and Oberbeck V. (1976) Cosmic ray exposure ages of Apollo 17 samples and the age of Tycho. *Proc. Lunar Sci.* **7,** 2817-2832.

Bischoff A. and Stöffler D. (1992) Shock metamorphism as a fundamental process in the evolution of planetary bodies: Information from meteorites. *Eur. J. Mineral.* **4,** 707-755.

Bogard D.D., Garrison D. H., and Nyquist L. E. (2000) Ar-39-Ar-40 ages of lunar highland rocks and meteorites (abstract). *Lunar and Planet. Sci.* **31,** 1138 (CD-ROM)

Bogard D. D., Garrison D. H., and McCoy T. J. (2000) Chronology and petrology of silicates from IIE iron meteorites: Evidence of a complex parent body evolution. *Geochim. Cosmochim.Acta* **64,** 2133-2154.

Carlson R.W and Lugmair G.W. (1988) The age of ferroan anorthosite 60025: Oldest crust on a young Moon. *Earth Planet. Sci. Lett.* **90,** 119-130.

Eugster O. and Michel T. (1995) Common asteroid break-up events of eucrites, diogenites, and howardites and cosmic-ray production rates for noble gases in achondrites. *Geochim. Cosmochim. Acta* **59,** 177-199.

Garrison D., Hamlin S., and Bogard D. (2000) Chlorine abundances in meteorites. *Met. and Planet. Sci.* **35,** 419-429.

Hartmann W. K. (2003) Megaregolith evolution and cratering cataclysm models – Lunar cataclysm as a misconception (28 years later). *Met. and Planet. Sci.* **38,** 579-593.

Karouji Y., Ebihara M., and Yamaguchi A. (2004) Chemical characteristics of lunar meteorites, Yamato 86032 and Dhofar 489 (abstract). *Antarct. Meteorites* **XXVIII,** 29-30.

Kieffer S. W. and Simonds C. H. (1980) The role of volatiles and lithology in the impact cratering process. *Rev. Geophys. Space Phys.* **18,** 143-181.

Koeberl C., Warren P. H., Lindstrom M. M., Spettel B., and Fukuoka T. (1989) Preliminary examination of the Yamato-86032 lunar meteorite: II. Major and trace element chemistry. *Proc. NIPR Symp. Antarct. Meteorites* **2,** 15-24.

Korotev R.L., Jolliff B. L., and Rockow K. M. (1996) Lunar meteorite Queen Alexandra Range 93069 and the iron concentration of the lunar highlands surface. *Met. and Planet. Sci.* **31,** 909-924.

Jacobsen S. B. and Wasserburg G. J. (1984) Sm-Nd isotopic evolution of chondrites and achondrites, II. *Earth Planet. Sci. Lett.* **67,** 137-150.

Lindstrom M.M. and Lindstrom D.J. (1986) Lunar granulites and their precursor anorthositic norites of the early lunar crust. *Proc. Lunar Planet. Sci. Conf.* **16,** D263-D276.

McDougall I. and Harrison T. M. (1999) *Geochronology and thermochronology by the $^{40}Ar/^{39}Ar$ method (2nd ed.)*. Oxford University Press, New York.

McKay D. S., Bogard D. D., Morris R. V., Korotev R. L., Johnson P., and Wentworth S. J. (1986) Apollo 16 regolith breccias: Characterization and evidence for early formation in the mega-regolith. *Proc. Lunar Planet. Sci. Conf.* **16,** D277-D303.

Misawa K., Tatsumoto M., Dalrymple G. B., and Yanai K. (1993) An extremely low U/Pb source in the Moon: U-Th-Pb, Sm-Nd, Rb-Sr, and 40Ar/39Ar isotopic systematics and age of lunar meteorite Asuka 881757. *Geochim. Cosmochim. Acta* **57,** 4687-4702.

Misawa K., Yamaguchi A., and Kaiden H. (2005) U-Pb and 207Pb-206Pb ages of zircons from basaltic eucrites: Implications for early basaltic volcanism on the eucrite parent body (in press). *Geochim. Cosmochim. Acta* **xx,** yyy-yyy.

Nielsen R.J. and Drake M.J. (1978) The case for at least three mare basalt magmas at the Luna 24 landing site. In: *Mare Crisium: The View from Lunar 24. (Ed. R. B. Merrill and J. J. Papike),* Pergamon, pp. 419-428.

Nyquist L. E. and Shih C.-Y. (2005) The lunar Rb/Sr ratio and implications for lunar history. *Meteorit. and Planet. Sci.* **40,** A116.

Nyquist L. E., Takeda H., Bansal B. M., Shih C.-Y., Wiesmann H., and Wooden J. L. (1986) Rb-Sr and Sm-Nd internal isochron ages of a subophitic basalt clast and a matrix sample from the Y75011 eucrite. *J. Geophys. Res.* **91,** 8137-8150.

Nyquist L. E., Bogard D. D., Wiesmann H., Bansal B. M., Shih C.-Y., and Morris R. M. (1990) Age of a eucrite clast from the Bholghati howardite. *Geochim. Cosmochim. Acta* **54,** 2197-2206.

Nyquist L. E., Wiesmann H., Bansal B., Shih C.-Y., Keith J.E., and Harper C. L. (1995) ^{146}Sm-^{142}Nd formation interval for the lunar mantle. *Geochim. Cosmochim. Acta* **59,** 2817-2837.

Nyquist L. E., Bogard D. D., and Shih C.-Y. (2001) Radiometric chronology of the Moon and Mars. In: *The Century of Space Science,* Kluwer Academic Publishers, pp. 1325-1376.

Nyquist L.E., Bogard D. D., Shih C.-Y., and Wiesmann H. (2002) Negative ε_{Nd} in anorthositic clasts in Yamato 86032 and MAC88105: Evidence for the LMO? (abstract) *Lunar Planet. Sci.* **33,** 1289, (CD-ROM).

Nyquist L. E., Shih C.-Y., and Takeda H. (2004) Chronology of eucrite petrogenesis from Sm-Nd and Rb-Sr systematics. *Antarct. Met.* **XXVIII,** 66-67.

Nyquist L.E., Yamaguchi A., Bogard D., Shih C.-Y., Reese Y., and Takeda H. (2005) Feldspathic clasts in Yamato 86032: Remnants of a feldspathic lunar crust 4.4 Ga ago. *Antarct. Met.* **XXIX,** 57-58.

Palme H., Spettel K., Jochum K. P., Dreibus G., Weber H., Weckwerth G., Wänke H., Bischoff A., Stöffler D. (1991) *Geochim Cosmochim Acta* **55,** 3105-3122.

Shih C.-Y., Nyquist L. E., Dasch E. J., Bogard D. D., Bansal B. M., and Wiesmann H. (1993) Ages of pristine noritic clasts from lunar breccias 15445 and 15455. *Geochim. Cosmochim. Acta* **57,** 915-931.

Solomon S. C. and Longhi J. (1977) Magma oceanography: 1. Thermal evolution. *Proc. Lunar Planet. Sci. Conf.* **8,** 583-599.

Stoenner R. W., Schaeffer O. A., and Katcoff S. (1965) Half-lives of argon-37, argon-39, and argon-42. *Science* **148,** 1325-1328.

Stöffler D. (1981) Cratering mechanics: data from terrestrial and experimental craters and implications for the Apollo 16 site (abstract). In: *Workshop on Apollo 16 (Ed. O. B. James and F. Hörz) LPI Tech. Rpt. 81-01,* pp. 132-141.

Takaoka N. and Yosida Y. (1992) Noble gases in Yamato-793274 and -86032 lunar meteorites. Proc. NIPR Symp. *Antarct. Met.,* **5,** 36-48.

Takeda H., Kojima H., Nishio F., Yanai K. Lindstrom M. M., and Yamato Lunar Meteorite Consortium Group (1989) Preliminary report on the Yamato-86032 lunar meteorite: I. Recovery, sample descriptions, mineralogy and petrography. *Proc. NIPR Symp. Antarct. Met.* **2,** 3-14.

Takeda H., Miyamoto M. Mori H., Wentworth S. J., and McKay D. S. (1990) Mineralogical comparison of the Y-86032-type Lunar Meteorites to Feldspathic Fragmental Breccia 67016. *Proc. Lunar Planet. Sci. Conf.* **20,** 91-100.

Takeda H., Nyquist L. E., and Kojima H. (2002) Mineralogical study of a gray anorthositic clast in the Yamato 86032 lunar meteorite: Windows to the far-side highland (abstract). *Lunar Planet. Sci.* **33,** 1267 (CD-ROM).

Tatsumoto M. and Premo W. R. (1991) U-Pb isotopic characteristics of lunar meteorites Yamato-793274 and Yamato-86032. *Proc. NIPR Symp. Antarct. Met.* 4, 56-69.

Tera F., Papanastassiou D. A. and Wasserburg G. J. (1974) Isotopic evidence for a terminal lunar cataclysm. *Earth Planet. Sci. Lett.* 22, 1-21.

Walker D. (1983) Lunar and terrestrial crust formation. *Proc. Lunar Planet. Sci. Conf.* **14,** B17-B25.

Warren P. H. and Wasson J. T. (1977) Pristine nonmare rocks and the nature of the lunar crust. *Proc. Lunar Planet. Sci. Conf.* **8,** 2215-2235.

Warren P. H. and Kallemeyn G. W. (1989) Elephant Moraine 87521: The first lunar meteorite composed of predominantly mare material. *Geochim. Cosmochim. Acta* **53,** 3323-3330.

Wasserburg G. J., Jacobsen S. B., DePaolo D. J., McCulloch M. T., and Wen T. (1981) Precise determination of the Sm/Nd ratios, Sm and Nd isotopic abundances in standard solutions. *Geochim. Cosmochim. Acta* 45, 2311-2323.

Yamaguchi A., Takeda H., Nyqusit L. E., Bogard D. D., Ebihara M., and Karouji Y. (2004) The origin and impact history of lunar meteorite Yamato 86032 (abstract). *Lunar Planet. Sci.* **31,** 1474 (CD-ROM).

Yamaguchi A., Takeda H., Nyquist L. E., Ebihara M., and Karouji Y. (2004) The origin and impact history of lunar meteorite Yamato 86032 (abstract). *Lunar Planet. Sci.* **35,** 1474 (CD-ROM).

Yamaguchi A., Takeda H., Karouji Y, Ebihara M., Nyquist L. E., Bogard D. D., Shih C.-Y., and Reese Y. (2005) Yamato-86032 Lunar meteorite: Implications for impact history of the highland crust (abstract). *Antarct. Met.* **XXIX,** 96-97.

APPENDIX 1: ^{37}Ar HALF-LIFE AND ^{39}Ar/^{37}Ar CORRECTION FACTORS

The complex, brecciated nature of Y-86032 combined with its anorthositic composition place stringent demands on radiometric dating techniques. For example, the ^{39}Ar-^{40}Ar dating technique is based on the reaction ^{39}K (n, p) ^{39}Ar. However, ^{39}Ar is also produced from the reaction ^{42}Ca (n, α) ^{39}Ar. Thus, a correction for Ca-produced ^{39}Ar must be applied. This is done by multiplying ^{37}Ar produced in the reactor from the reaction ^{40}Ca (n, p) ^{37}Ar by a ^{39}Ar/^{37}Ar factor experimentally determined for the reactor used. Corrections to ^{39}Ar of 25-50% are typical for samples with K/Ca ratios <0.001, like lunar anorthosites. Yet, many earlier reports of Ar-Ar ages of lunar anorthosites did not discuss uncertainties in the ^{39}Ar corrections that were applied. It is well known that the ^{39}Ar/^{37}Ar correction factor varies among neutron reactors, but the extent of the variation among different irradiations in the same reactor apparently has not been investigated in detail . Further, because ^{37}Ar decays rapidly, the measured ^{37}Ar must be corrected back to the time of irradiation, and any uncertainty in the ^{37}Ar half-life affects the correction to ^{39}Ar, and thus the age. Measurements of the ^{37}Ar half-life reported in the literature were all determined by counting the rate of ^{37}Ar decay, and vary by a few percent. Although most labs that determine Ar-Ar ages use a half-life of 35.1 days as reported by Stoenner et al. (1965), past publications of the Chart of the Nuclides have given various half-lives representing averages of different determinations.

In order to accurately determine the ^{39}Ar/^{37}Ar correction factor for our low-K samples, to confirm the ^{37}Ar half-life by a non-counting technique, and to examine possible variations in the ^{39}Ar/^{37}Ar correction factor among different irradiations in the same reactor, we included two samples of a pure CaF_2 crystal in each of five neutron irradiations made over a period of five years. Each irradiation was conducted in the same insertion port location of the University of Missouri Research Reactor (MURR). For each sample in a pair of CaF_2 samples, we measured the Ar isotopic composition at different times after irradiation. The difference in measured ^{39}Ar/^{37}Ar ratios in these sample pairs depends solely on the decay of ^{37}Ar. (A correction is applied for the decay of ^{39}Ar, but this is very minor). Thus, precise measurements of the ^{39}Ar/^{37}Ar ratio by mass spectrometry gives a determination of the ^{37}Ar half-life by a

technique completely different from the counting techniques previously used, as well as the $^{39}Ar/^{37}Ar$ correction factor that must be applied to the meteorite data.

A1.1 Half-life of ^{37}Ar.

The measured $^{39}Ar/^{37}Ar$ ratios, calculated ^{37}Ar half-life, and determined $^{39}Ar/^{37}Ar$ correction factors for the five pairs of CaF_2 samples are given in Table A1. Uncertainties listed for the $^{39}Ar/^{37}Ar$ factors include errors in measured isotopic ratios and blank corrections. Time differences between analyses (Δ-T) of each CaF_2 sample in a pair varied between 57 and 102 days, approximately 2 to 3 half-lives of ^{37}Ar. This time was used to decay-correct the $^{39}Ar/^{37}Ar$ ratio for the second sample in each pair to match the $^{39}Ar/^{37}Ar$ ratio of the first sample in each pair. In this correction, the value of the ^{37}Ar half-life was considered a variable, and the half-life values listed in Table A1 are those required to match $^{39}Ar/^{37}Ar$ ratios for each pair of CaF_2 samples. The five half-life determinations show a tight grouping and give an average value of 35.06 ±0.04 (1σ) days. This value is the same within respective uncertainties of the ^{37}Ar half-life of 35.1 ±0.1 days reported by Stoenner et al. (1965).

Table A1. Data determined from pairs (#1 & #2) of irradiated CaF_2 samples.

Irrad. No.	Δ-T (days)	Measured $^{39}Ar/^{37}Ar$ & ± (x10^4) #1	#2	^{37}Ar $t^1/_2$ (days)	$^{39}Ar/^{37}Ar$ Factor x10^4
97A	100	519.29 ±0.26	77.742 ±0.033	35.06	7.495 ±0.078
98A	76	873.39 ±0.56	193.75 ±0.13	35.10	7.364 ±0.074
99C	57	346.41 ±0.55	108.50 ±0.11	35.01	7.681 ±0.077
00A	102	915.80 ±1.18	121.19 ±0.15	35.02	7.104 ±0.137
02A	93	519.29 ±0.26	77.742 ± 0.033	35.10	7.495 ±0.075

A1.2 Variability in $^{39}Ar/^{37}Ar$ Factors.

The average $^{39}Ar/^{37}Ar$ correction factor for these five irradiations is 7.43 ±0.21 x10^{-4}, which becomes 7.51 ±0.13 x10^{-4} if we omit the value for sample 00A, which is considerably lower than the others and possesses the largest uncertainty. Although ^{37}Ar half-lives derived from the five pairs of CaF_2 samples show a spread of only 0.26%, the determined $^{39}Ar/^{37}Ar$ correction factors show a total spread of 7.7%, which is considerably larger than the individual uncertainty of ~1% for four of the five factors. The larger variation is thus produced by different irradiations, not by a variation among individual

samples, and is not explained by variable K contamination on the surface of the CaF_2, as suggested by McDougall and Harrison (1999).

Each $^{39}Ar/^{37}Ar$ factor in Table A1 was calculated by forcing the $^{39}Ar/^{37}Ar$ ratio for the two samples in each CaF_2 pair to be equal, and thus assumes the ^{37}Ar half-life has the value determined for that irradiation. If, instead, we use the average determined ^{37}Ar half-life of 35.06 d, the difference in $^{39}Ar/^{37}Ar$ correction factors for the two CaF_2 samples in each pair still remains small compared to the difference among $^{37}Ar/^{39}Ar$ factors reported in Table A1 for each pair. To force the $^{39}Ar/^{37}Ar$ factors for the five irradiations to be equal would require significant variations in the actual ^{37}Ar half-life, which cannot be true. Thus, we conclude that these irradiations actually give slightly different values of the $^{37}Ar/^{39}Ar$ correction factor, in spite of the fact that the irradiations were conducted in a similar manner. We believe that we can discount several specific factors as causes for the observed $^{39}Ar/^{37}Ar$ variation. First, the ^{37}Ar decay correction applied for each irradiation includes decay of ^{37}Ar during the irradiation, in addition to ^{37}Ar decay after the irradiation. Secondly, samples in each CaF_2 pair were irradiated in adjacent positions within the same quartz tube, except sample 98A, where the two samples were irradiated in the same relative positions of adjacent quartz tubes. Further, irradiations 97A-99C were made with boron-nitride shielding around the samples to adsorb thermal neutrons, whereas the irradiations 00A and 02A had no thermal shielding. (We would not expect changes in thermal neutron flux to affect the neutron rigidity in the MeV energy range.)

We believe that the variable $^{39}Ar/^{37}Ar$ correction factors can be explained by characteristics of reactor operation. The excitation functions (i.e., cross section as a function of energy) for production of ^{39}Ar and ^{37}Ar by neutron capture on Ca are not identical. Thus, the specific $^{39}Ar/^{37}Ar$ correction factor also depends upon neutron rigidity, i.e., the flux of fast neutrons as a function of energy. Among various reactors that have been used for $^{39}Ar/^{40}Ar$ dating, correction factors of ~(6.4-12) $x10^{-4}$ have been reported (McDougall and Harrison, 1999). The MURR reactor contains eight fuel elements in a cylindrical array, and periodically one fuel element at a time is replaced. (Fission products build up in old fuel elements and slow down the chain reaction by adsorbing neutrons.) Control rods are used to maintain a constant

thermal neutron flux during each 6.5-day neutron-generating cycle. Our irradiation position is located on the outside edge of the reactor core. Thus, depending on whether the nearest fuel element to our irradiation position is new or old, and on the relative position of the control rods in the core, the neutron rigidity can vary at our irradiation location. We believe this is the explanation for the observed ~8% variation in $^{39}Ar/^{37}Ar$ correction factors in Table 1. We point out that such variations are likely to occur in all reactors, and thus any analysis of samples with very low K/Ca ratios should document such variations, and not simply assume that one value determined for a given reactor is invariant.

Because we did not include CaF_2 samples in every University of Missouri irradiation that contained low-K samples, we adopt a standard $^{39}Ar/^{37}Ar$ correction factor of $7.5 \pm 0.2 \times 10^{-4}$ for the sample analyses reported here. We believe these procedures have improved both the precision and accuracy of the Ar-Ar ages of the various Y-86032 lithologies.

Table 1a. The Sm isotopic results for lunar meteorite Y-86032. (normalized to $^{148}Sm/^{154}Sm=0.49419$)

sample	wt.(mg)	$^{147}Sm/^{154}Sm$[b]	$^{149}Sm/^{154}Sm$	$^{150}Sm/^{154}Sm$	$^{152}Sm/^{154}Sm$
Y-86032,28 LG (Light-Gray lith.) (2 runs)					
WR[a,c,e]	26.25	0.659222±58	0.607408±21	0.324435±57	1.175458±244
		(*0.77±0.88*	*-0.81±35*	*1.16±1.77*	*0.79±2.08*)
Y-86032,133 WC (White Clast) (2 runs)					
WR	35.35	0.659240±12	0.607402±15	0.324473±34	1.175374±18
		(*1.04±0.18*	*-0.93±0.25*	*2.33±1.05*	*0.08±0.15*)
Y-86032,43 (Dark-Gray lith.) (3 runs)					
WR	26.00	0.659259±158	0.607397±46	0.324485±20	1.175364±31
		(*1.33±2.40*	*-1.00±0.76*	*2.70±0.62*	*-0.01±0.27*)
Y-86032,44 DG (Dark-Gray lith.) (4 runs)					
WR	24.30	0.659244±60	0.607421±24	0.324452±18	1.175313±69
		(*1.10±0.91*	*-0.61±0.39*	*1.70±0.54*	*-0.44±0.58*)
Y-86032,30 IM (Impact Melt) (2 runs)					
WR	29.05	0.659198±38	0.607374±11	0.324450±23	1.175405±82
		(*0.40±0.58*	*-1.37±0.17*	*1.63±0.70*	*0.34±0.70*)
Y-86032,37 IM (Impact Melt) (1 run)					
WR	30.40	0.659492	0.607374	0.324430	1.175473
		(*4.86*	*-1.37*	*1.00*	*0.92*)
Y-86032,33 IM (Impact Melt) (5 runs)					
WR	33.00	0.659249±89	0.607368±39	0.324448±50	1.175255±135
		(*1.18±1.36*	*-1.48±0.64*	*1.55±1.55*	*-0.93±1.15*)
Ames Sm standard[d] :					
(16 analyses; 10/05)		0.659171±66	0.607458±44	0.324397±38	1.175365±64

Table 1b. The Sm isotopic results for lunar meteorite Y-86032,116. (normalized to $^{147}Sm/^{152}Sm=0.56081$)

sample	wt.(mg)	$^{148}Sm/^{152}Sm$[b]	$^{149}Sm/^{152}Sm$	$^{150}Sm/^{152}Sm$	$^{154}Sm/^{152}Sm$
Y-86032,116 GC (average of 2 runs)					
WR[a,c,e]	25.2	0.421025±149	0.516872±21	0.276063±3	0.851151±137
		(*13.1±3.5*	*-0.66±0.41*	*0.90±0.11*	*0.40±1.61*)
Ames Sm standard[d] :					
(2 analyses; 11/01)		0.420476±42	0.516906±30	0.276038±20	0.851117±15

[a]WR=whole rock.
[b]Normalized to $^{148}Sm/^{154}Sm=0.49419$ or $^{147}Sm/^{152}Sm=0.56081$ (Wasserburg *et al.*, 1981) and use the exponential law for mass fractionation corrections.
[c]Uncertainties correspond to last figures and represent $\pm 2\sigma_m$ error limits.
[d]Uncertainties correspond to last figures and represent $\pm 2\sigma_p$ error limits.
[e]italics are ε-values of respective isotopic ratios relative to the Sm standard.
[e]italics are ε-values of respective isotopic ratios.

Table 2. The Sm-Nd analytical results for lunar meteorite Y-86032.

sample	wt.(mg)	Sm(ppm)	Nd(ppm)	$^{147}Sm/^{144}Nd$[b]	$^{143}Nd/^{144}Nd$[b,c]	T_{Ar-Ar} (Ga)	εNdi
Y-86032,116 GC							
WR[a]	16.30	0.2280	0.7993	0.17250±27	0.511094±14	4.40±0.05	-0.92±0.32
Y-86032,116 Matrix							
WR	18.50	0.4360	1.570	0.16801±17	0.511188±10		
Ames Nd standard :			Nd^+	(7 analyses 12/95) :	0.511105±14[d]		
			NdO^+	(4 analyses 12/95) :	0.511087±26[d]		
Y-86032,28 LG (Light-Gray lith.)							
WR	20.70	0.3400	1.177	0.17464±23	0.511200±10		
Plag	15.01	--------	-------				
Px1	3.85	0.929	2.688	0.20903±43	0.512217±10		
Px2	2.05	1.398	3.064	0.27601±71	0.514174±19		
Y-86032,33 IM (Impact melt)							
WR	21.40	0.5733	1.901	0.18236±20	0.511376±10		
Y-86032,44 (Dark-Gray lith.)							
WR	23.25	0.6566	2.118	0.18750±20	0.511592±10		
Plag	14.3	0.4886	1.686	0.17527±20	0.511227±11		
Px1	4.55	0.8670	2.569	0.20412±26	0.512078±10		
Px2	1.30	0.7140	1.738	0.24840±91	0.513388±10		
Ames Nd standard :			NdO^+	(12 analyses 5/04) :	0.511099±19[d]		
			NdO^+	(11 analyses 11-12/04) :	0.511121±16[d]		
			NdO^+	(9 analyses 2/05) :	0.511122±11[d]		

[a]WR=whole rock, Plag=plagioclase, Px1=pyroxene+plagioclase, Px2=pyroxene.
[b]Uncertainties correspond to last figures and represent $\pm 2\sigma_m$ error limits.
[c]Normalized to $^{146}Nd/^{144}Nd=0.724140$ and adjusted to $^{143}Nd/^{144}Nd=0.511138$ of the Ames Nd standard (Wasserburg *et al.*, 1981).
[d]Uncertainties correspond to last figures and represent $\pm 2\sigma_p$ error limits.
[e]Nd runs as Nd^+ mode.

Table 3. The Rb-Sr analytical results for lunar meteorite Y-86032.

sample	wt.(mg)	Rb(ppm)	Sr(ppm)	$^{87}Rb/^{86}Sr$[b]	$^{87}Sr/^{86}Sr$[b,c]	T_{Ar-Ar} (Ga)	$(^{87}Sr/^{86}Sr)_i$
Y-86032,116 GC							
WR	16.30	0.117	159.8	0.00211±2	0.699213±20	4.40±0.05	0.699079±20
Y-86032,116 Matrix							
WR	18.50	0.289	157.4	0.00532±3	0.699429±11		
NBS 987 Sr standard:		Sr^+	(12 analyses 12/1995) :		0.710249±34[d]		
Y-86032,28 LG lith.							
WR	20.70	0.0747	178.9	0.00121±2	0.699135±10		
Plag	15.01	0.0901	238.1	0.00109±2	0.699120±10		
Px1	3.85	0.0624	126.6	0.00143±3	0.699149±10		
Px2	2.05	0.0278	15.69	0.00513±46	0.699257±12		
Y-86032,33 Impact melt							
WR	21.40	0.3800	154.7	0.00711±8	0.699475±10		
Y-86032,44 DG lith.							
WR	23.25	0.2854	143.5	0.00576±5	0.699460±10		
Plag	14.3	0.2974	182.9	0.00471±5	0.699380±10		
Px1	4.55	0.2521	113.0	0.00646±8	0.699534±10		
Px2	1.30	0.0829	22.78	0.0105±5	0.699883±10		
NBS 987 Sr standard:		Sr^+	(3 analyses 6/2004) :		0.710231±26[d]		
		Sr^+	(2 analyses 6/2004) :		0.710254±16[d]		
		Sr^+	(9 analyses 12/2004) :		0.710240±32[d]		
		Sr^+	(28 analyses 2/2005) :		0.710250±30[d]		

[a]WR=whole rock, Plag=plagioclase, Px1=pyroxene+plagioclase, Px2=pyroxene.
[b]Uncertainties correspond to last figures and represent $\pm 2\sigma_m$ error limits.
[c]Normalized to $^{88}Sr/^{86}Sr=8.37521$ and adjusted to $^{87}Sr/^{86}Sr=0.710250$ of the NBS 987 Sr standard (Nyquist *et al.*, 1990).
[d]Uncertainties correspond to last figures and represent $\pm 2\sigma_p$ error limits.

FIGURE CAPTIONS

Fig.1.

Y-86032 slab from which samples were allocated for this investigation. Four lithologies were identified: White anorthositic or granulitic clasts (W), light gray anorthositic breccia (LG), dark gray regolithic breccia (DG), and black impact melt (IM). The sampled areas are outlined in blue. See Fig. 5 for a summary of the isotopic analyses for individual allocations. The relationships of IM and DG to LG within the outlined rectangular area are shown in more detail in the photomicrograph of Fig. 2.

Fig. 2.

Photomicrograph of Y-86032 showing the textures and relationships of the light gray (LG), dark gray (DG), and impact melt (IM) lithologies. Note that a fragment of the light gray (LG) lithology has broken away and has been surrounded by the dark gray (DG) lithology. Note also that the impact melt (IM) smoothly abuts both lithologies. Mineral clasts occur scattered throughout both the DG and IM lithologies.

Fig. 3.

CI-normalized REE abundances of representative samples of the Y-86032 lithologies. INAA and ICPMS data for LG are from allocation ,28, a split of the sample used for isotopic studies. Data for 131 DG, 34 IM, and 36 IM are reported in Karouji et al. (2004).

Fig. 4.

FeO-Th diagram of Y-86032 from data reported by Karouji et al. (2004). Sample allocations for LG, DG, and IM are identified in Fig. 3. Compositional ranges for the Apollo samples are shown as shaded areas as given by Korotev et al. (1996). Note the extremely low Th content of Y-86032 which establishes its origin as far distant from the Procellarum KREEP Terrain (PKT). The FeO abundance of this brecciated lithology is among the lowest observed for lunar feldspathic samples.

Fig.5.

Y-86032 allocations for isotopic studies.

Fig. 6.

Sm isotopic composition of Y-86032 subsamples. Although the data are tightly clustered, nearly overlapping within analytical uncertainty, three samples (,116GC ,28LG and ,44DG) cluster to the right on the diagram (lowest neutron exposure) and three samples (,30 IM ,33 IM and ,30 IM) cluster to the left (highest neutron exposure). Note that the subsample of allocation ,30 DG that was analysed for Sm isotopes was enriched in impact melt, and is here designated IM. Those samples most enriched in light-colored, feldspathic clasts appear to have the lowest exposure to thermal neutrons, and, thus, the shortest regolith residence time. Sample heterogeneity probably is an important factor, especially for the DG lithology (*cf.* Fig. 2). Note that ,44DG from which minerals were separated for the Sm-Nd isochron, is among those samples showing the lowest neutron exposure. Thus, the comparatively large mineral clasts separated from this regolith sample were nevertheless relatively pristine with respect to exposure in a regolith environment.

Fig. 7.

Mineral separation scheme for light gray, feldspathic sample ,28 LG. Note that ,28 Px2, the purest pyroxene fraction, constituted ~5% by mass of the total processed through separation. This amount compares favorably to the modal abundance of large pyroxene grains in the sample.

Fig. 8.

Sm and Nd abundances in mineral separates compared to those in bulk samples and to the overall REE abundance patterns of Y-86032 lithologies and Apollo FANs. Sm and Nd data for bulk samples are shown as light (yellow) circles, whereas those in mineral separates are shown as dark (red) squares. REE abundance patterns are calculated from data presented by Karouji et al. (2004). Apollo sample data are from the literature. Note that pyroxene separates from both ,28LG and ,44DG show the characteristic LREE depletion of pyroxene. Nd abundances for ,44 Plag and ,44Px2 are nearly identical. Analysis of the ,28 Plag sample failed.

Fig. 9.

Sm-Nd isochron for Y-86032,28LG and Y-86032,44DG (combined). As expected, the "Px 2" analyses of both samples plot at comparatively high $^{147}Sm/^{144}Nd$ ratios. Separated plagioclase from ,44DG and ,28LG plot at the lowest $^{147}Sm/^{144}Nd$ ratios. Although analysis of ,28 Plag failed, this probably is of little consequence for the isochron, since the ,28 bulk sample is ~95% plagioclase. The data for all analyses are colinear within the error limits of ~0.3 ε-units suggesting that the analysed minerals came either from a single lithic precursor, or more likely, from cogenetic lithologies. Thus, we interpret the isochron age, 4.43±0.03 Ga, as the age of crystallization of a primary crustal lithology or, possibly, a range of cogenetic lithologies. The initial ε_{Nd} value of Y-86032 is slightly positive relative to CHUR (Jacobsen and Wasserburg, 1984), but is distinctly negative relative to initial ε_{Nd} in eucritic meteorites (Nyquist et al., 2004). Thus, these samples of the lunar highlands crust could have crystallized from a feldspar-rich lunar magma ocean evolved from "chondritic" relative REE abundances as determined from eucrites.

Fig. 10.

Rb-Sr data for Y-86032 subsamples in comparison to those for some Apollo 16 FANs. A least-squares fit to colinear data for the FANs and Y-86032 gives a whole rock age of 4.62±0.89 Ga and initial $^{87}Sr/^{86}Sr$ (I(Sr)) = 0.699066±43. The Apollo 16 data apply to the near-side lunar crust, whereas the Y-86032 data probably apply to the far-side crust. Although the crustal formation age is imprecisely defined by these data, the initial $^{87}Sr/^{86}Sr$ ratio in the crust at the time of its solidification is relatively precisely defined. A tie-line through LG ,28 bulk rock and the IM ,33 impact melt gives an apparent age of 4.00±0.17 Ga, an estimate of the time the impact melt formed. The data for the pyroxene samples appear to be disturbed. We attribute this either to weathering in the Antarctic environment, or possibly to enhanced processing blanks for these mg-sized samples. Thus, we give no time significance to those data. The analysis of the 21-mg sample ,33 IM, however, is robust (Table 3). Thus, its displacement from the alignment of other robust analyses is significant. No mixing end member that could explain the high Rb/Sr ratio of the

impact melt has been identified. Thus, we tentatively attribute the higher Rb/Sr ratio of ,33 IM to partitioning of Rb into the melt during impact melting. In this case, the tie-line between it and ,28 Plag giving an apparent age of 4.00±0.17 Ga is a probable upper bound to the time of the melting event.

Fig. 11.

^{39}Ar-^{40}Ar ages (rectangles, left scale) and K/Ca ratios (stepped line, right scale) versus cumulative release of ^{39}Ar for stepwise temperature release of Y-86032,116GC. Width of the age rectangles indicate analytical age uncertainties, not considering the uncertainty in J.

Fig. 12.

^{39}Ar-^{40}Ar ages (rectangles, left scale) and K/Ca ratios (stepped line, right scale) versus cumulative release of ^{39}Ar for stepwise temperature release of Y-86032,28 LG.

Fig. 13.

^{39}Ar-^{40}Ar ages (rectangles, left scale) and K/Ca ratios (stepped line, right scale) versus cumulative release of ^{39}Ar for stepwise temperature release of Y-86032,33 IM. Two age spectra are shown. The older age spectrum (bold rectangles) has no correction applied for trapped ^{40}Ar. The lower age spectrum (light rectangles) is the result of correcting for trapped ^{40}Ar by assuming trapped ^{40}Ar/^{36}Ar =10.

Fig. 14.

^{39}Ar-^{40}Ar ages (rectangles, left scale) and K/Ca ratios (stepped line, right scale) versus cumulative release of ^{39}Ar for stepwise temperature release of Y-86032,30 (LG+IM). Two age spectra are shown. The older age spectrum (bold rectangles) has no correction applied for trapped ^{40}Ar. The lower age spectrum (light rectangles) is the result of correcting for trapped ^{40}Ar by assuming trapped ^{40}Ar/^{36}Ar =10.

Fig. 15.

Initial ε_{Nd} values for FANs, KREEP, and Y-86032 normalized to values that would exist in a “chondritic” reservoir as determined from measurements of many eucrites in the JSC lab (Nyquist et al., 2004). The

pararameters of this reservoir determine initial $^{143}Nd/^{144}Nd$ as shown by “HED PB” at 4.567 Ga ago. $^{143}Nd/^{144}Nd$ for HED PB are higher than our interlaboratory-adjusted value for CHUR (Jacobsen and Wasserburg, 1984) by 0.8 ε-units. The lunar data shown are from the JSC lab except for the age of 60025 (Carlson and Lugmair, 1988). The new data for the (,28 + ,44) combined isochron are consistent with radiogenic growth with $^{147}Sm/^{144}Nd$ = 0.17 from HED PB at 4.56 Ga ago. The earlier data for ,116 GC, plotted at the ^{39}Ar-^{40}Ar age of ,116 GC lie somewhat below this evolution line. The datum for ,33IM is shown plotted at the Rb-Sr tie-line age of 4.00±0.17 Ga (Fig. 10).

Fig. 16.

Rb-Sr isotopic data for Y-86032 and plagioclase separates from Apollo 16 FANs as analysed in the JSC lab and compared to data for CAI E38 and plagioclases from several eucrites (Nyquist et al., 2004). The Y-86032 data are very consistent with the Apollo 16 data, suggesting that the anorthositic lunar crust is isotopically homogeneous. See text for comparison to the CAI and eucrite data.

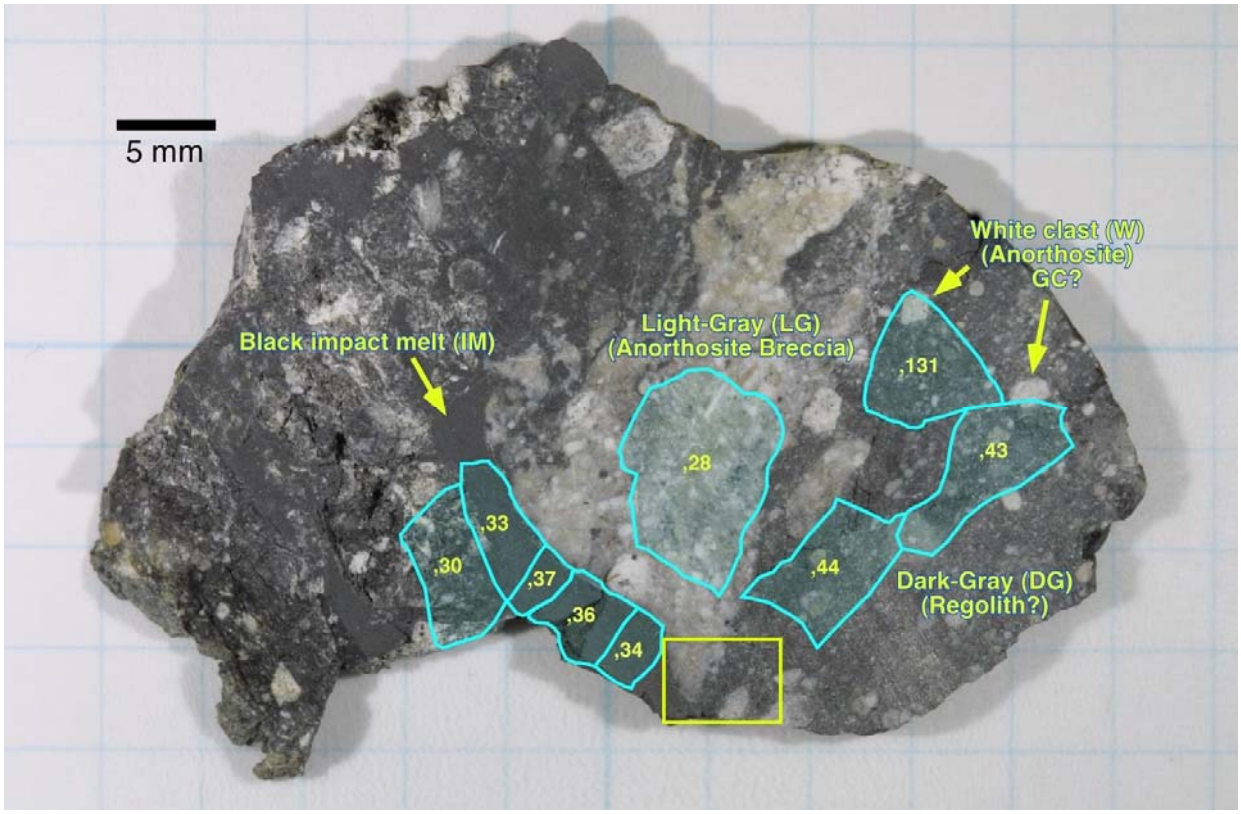

Figure 1

Nyquist et al.

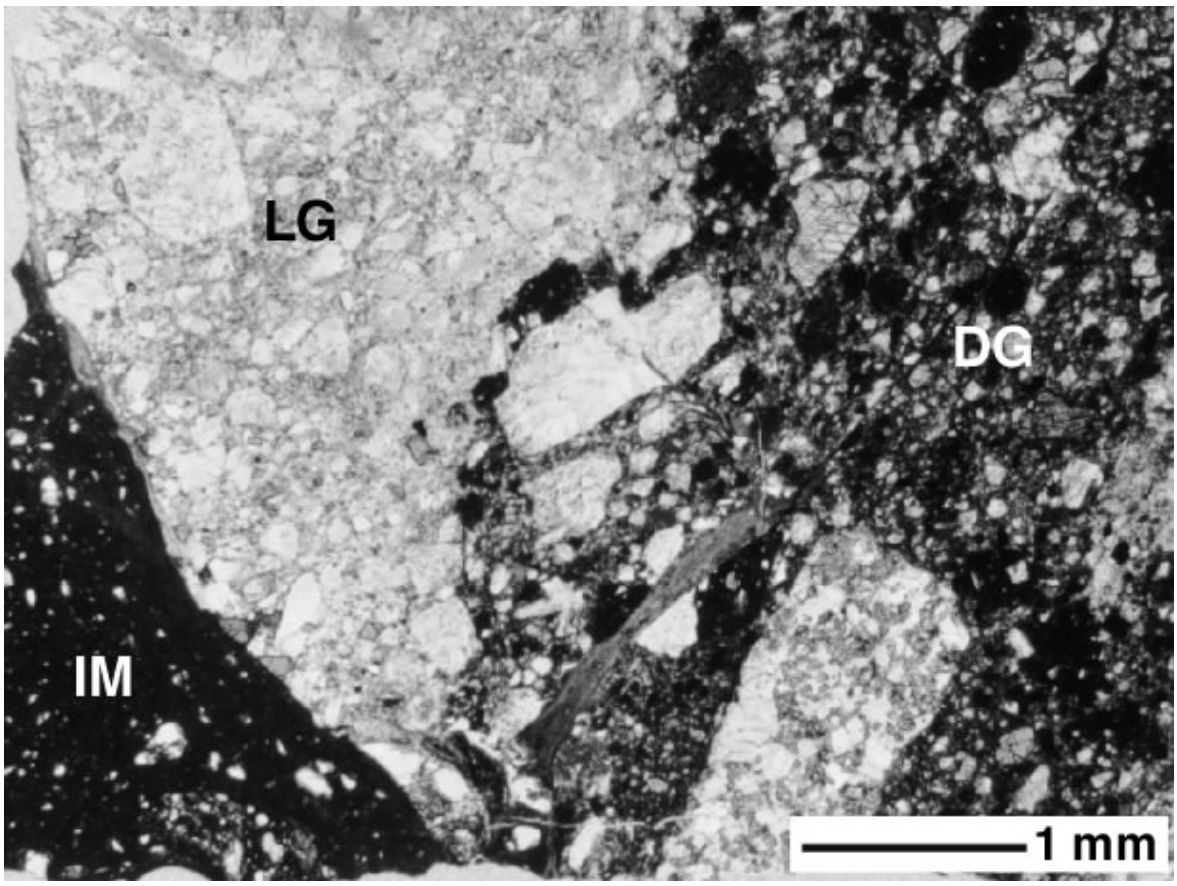

Figure 2

Nyquist et al.

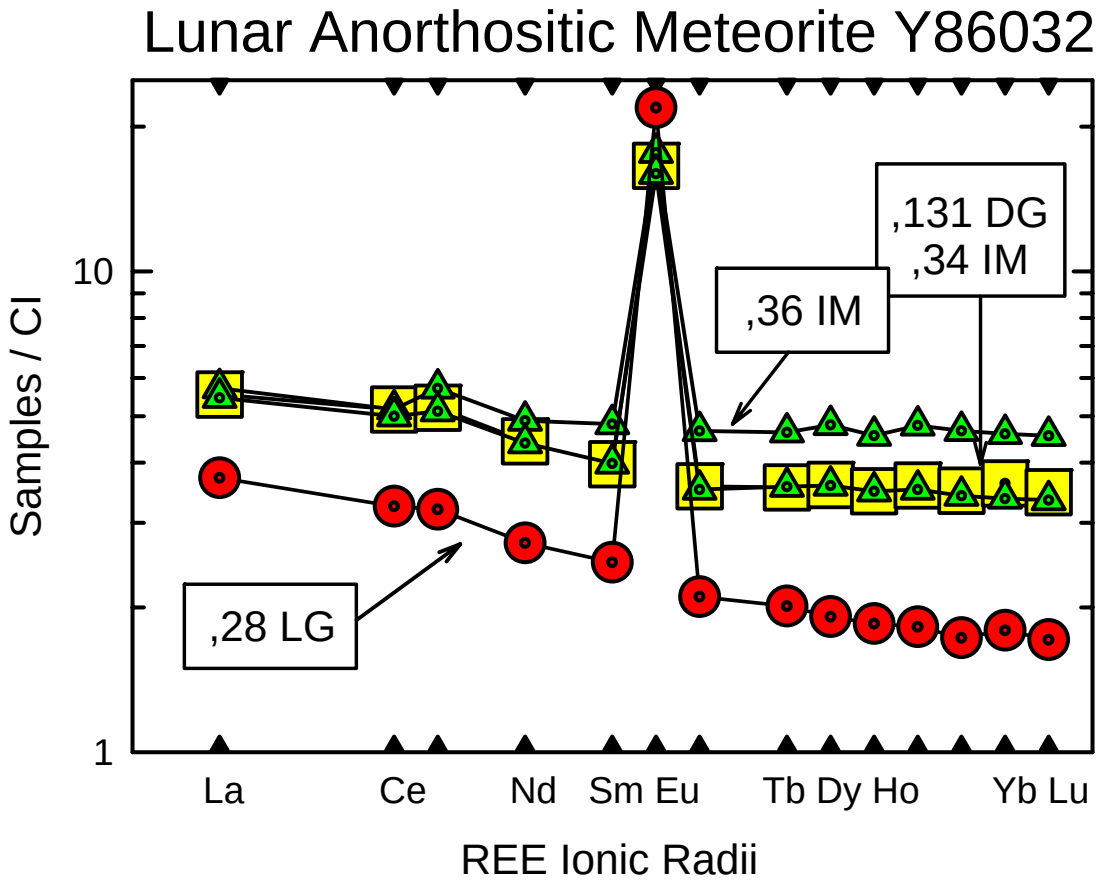

Figure 3

Nyquist et al.

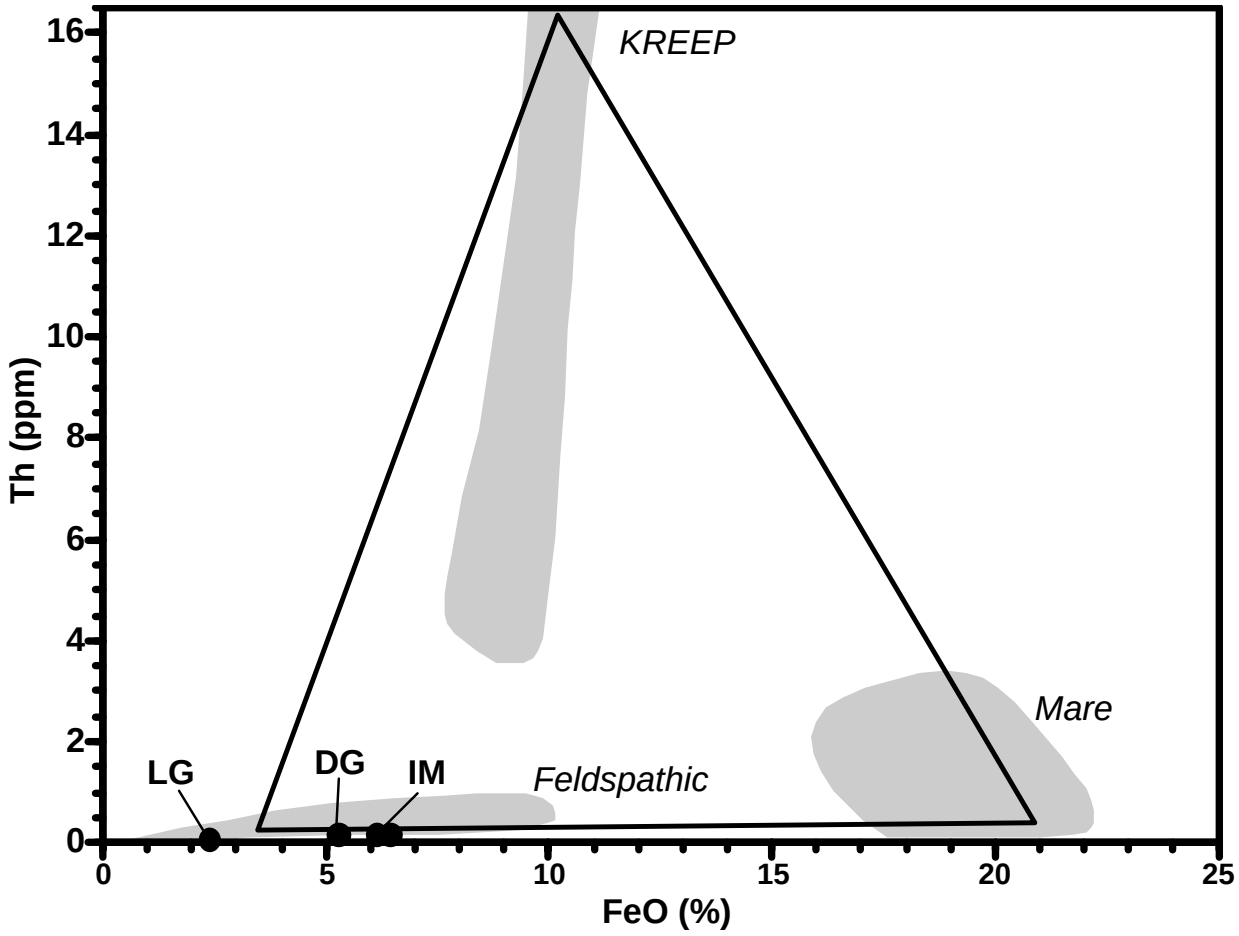

Figure 4

Nyquist et al.

- **Light colored clast from earlier allocation (,116 GC)**
  - **Ar-Ar: Whole rock (Bogard et al., 2000)**
  - **Rb-Sr, Sm-Nd: Whole rock (Nyquist et al., 2002)**
- **White (W) lithology (,133)**
  - **Sm-isotopes**
- **Light-gray (LG) lithology (,28)**
  - **Sm-isotopes**
  - **Ar-Ar: Whole rock**
  - **Rb-Sr, Sm-Nd:**
    - **Whole rock (homogenized, <149 μm powder)**
    - **Plag- and px-enriched separates, <74μm**
    - **4 samples *in toto***
- **Dark-gray (DG) lithology (,43 ,44)**
  - **Sm-isotopes**
  - **Ar-Ar: Whole rock (in work)**
  - **Rb-Sr, Sm-Nd:**
    - **Whole rock (homogenized, <149 μm powder)**
    - **Plag- and px-enriched separates, <74μm**
    - **4 samples *in toto***
- **Impact melt (IM) lithology (,33 ,37)**
  - **Sm-isotopes**
  - **Ar-Ar: Whole rock**
  - **Rb-Sr, Sm-Nd: Whole rock**

Figure 5

Nyquist et al.

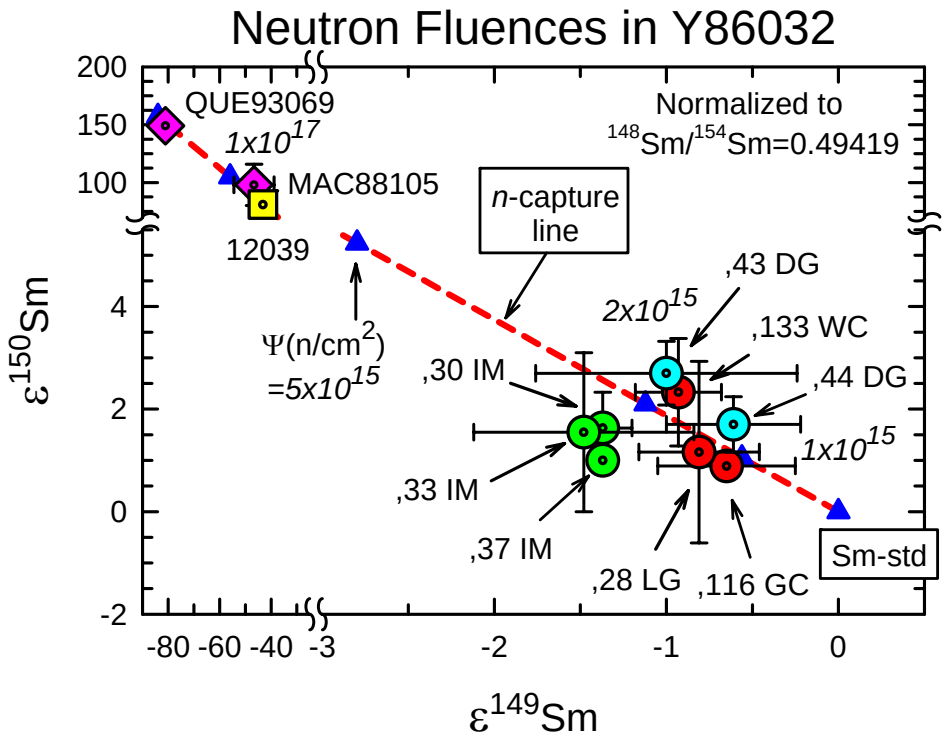

Figure 6

Nyquist et al.

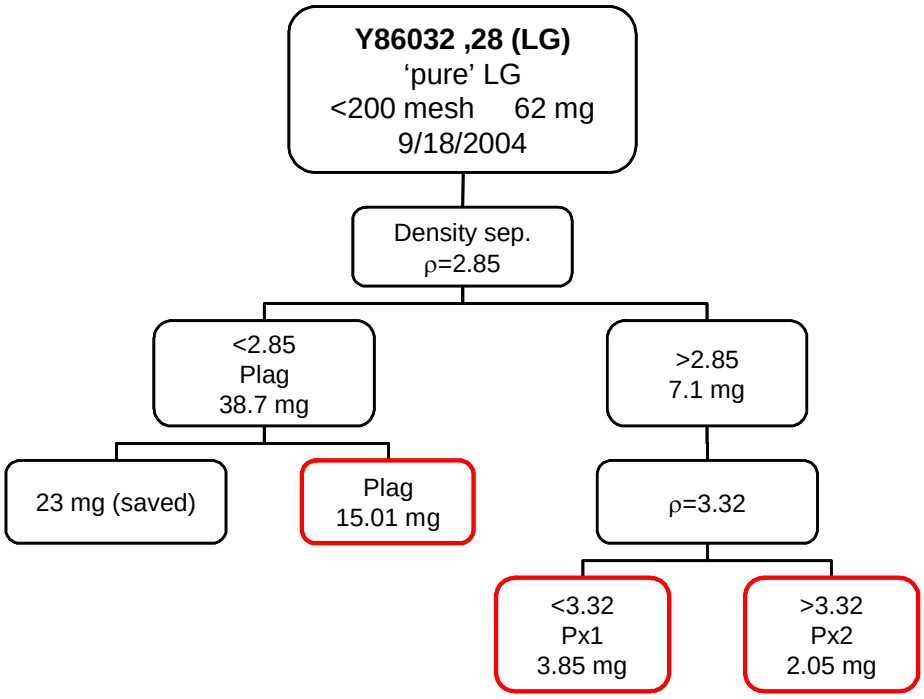

Figure 7

Nyquist et al.

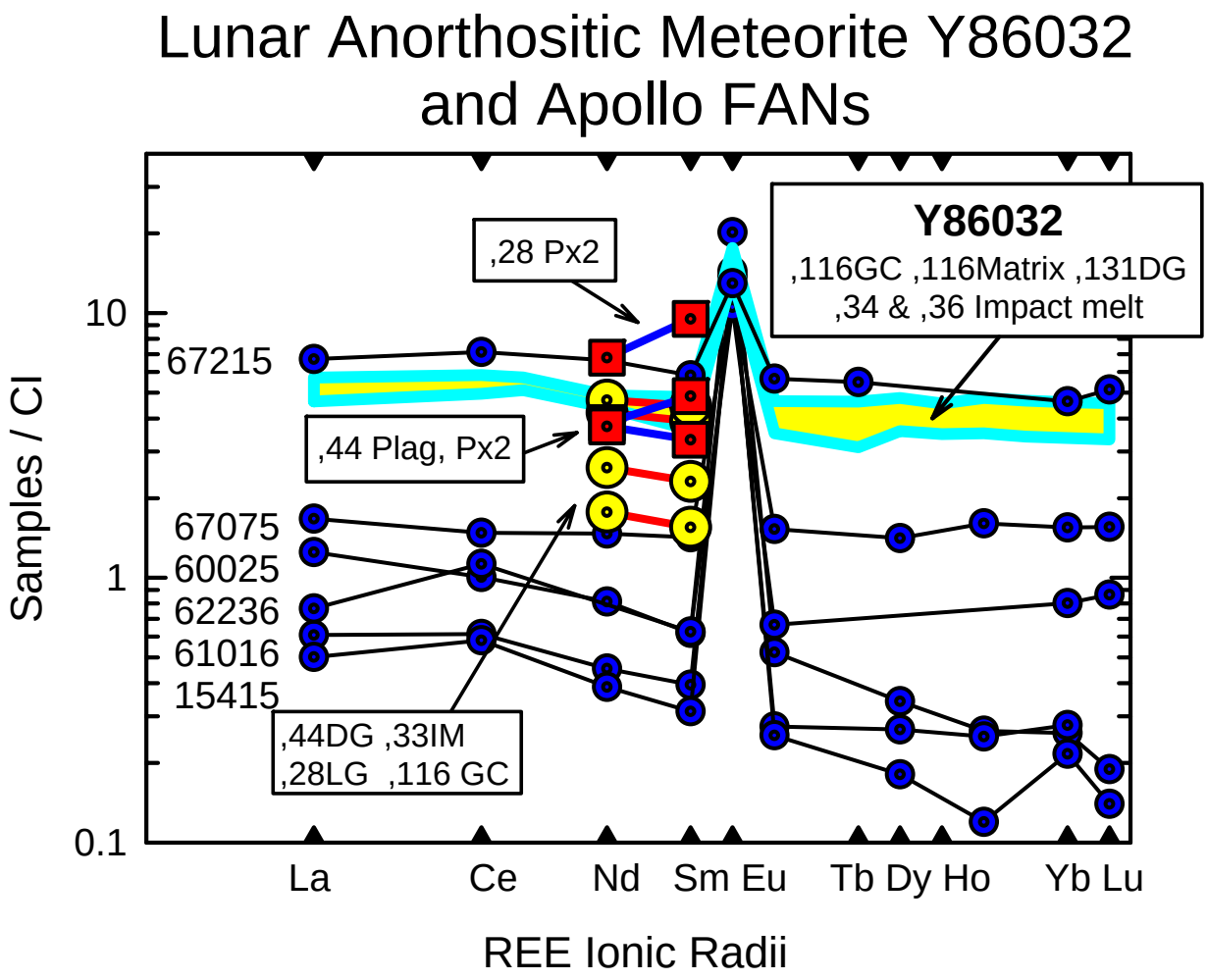

Figure 8

Nyquist et al.

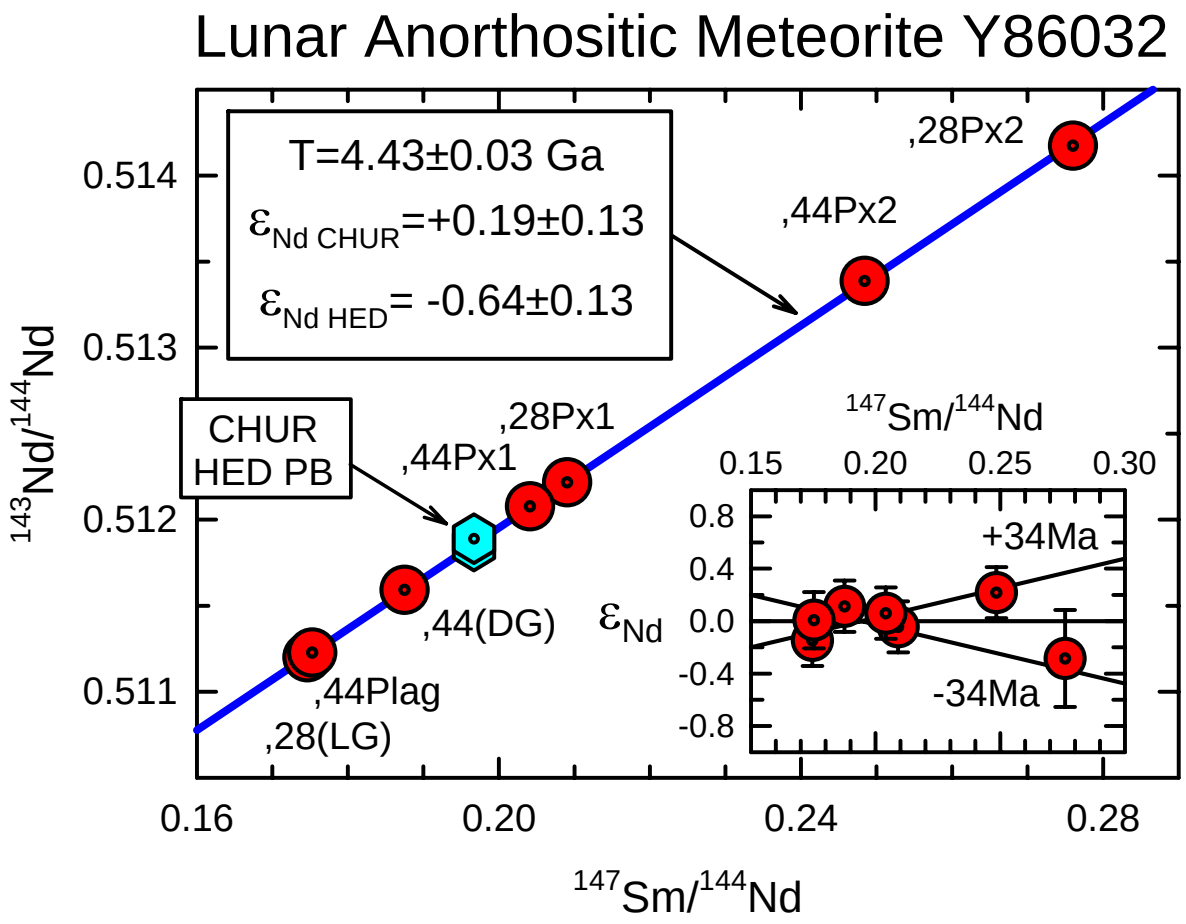

Figure 9

Nyquist et al.

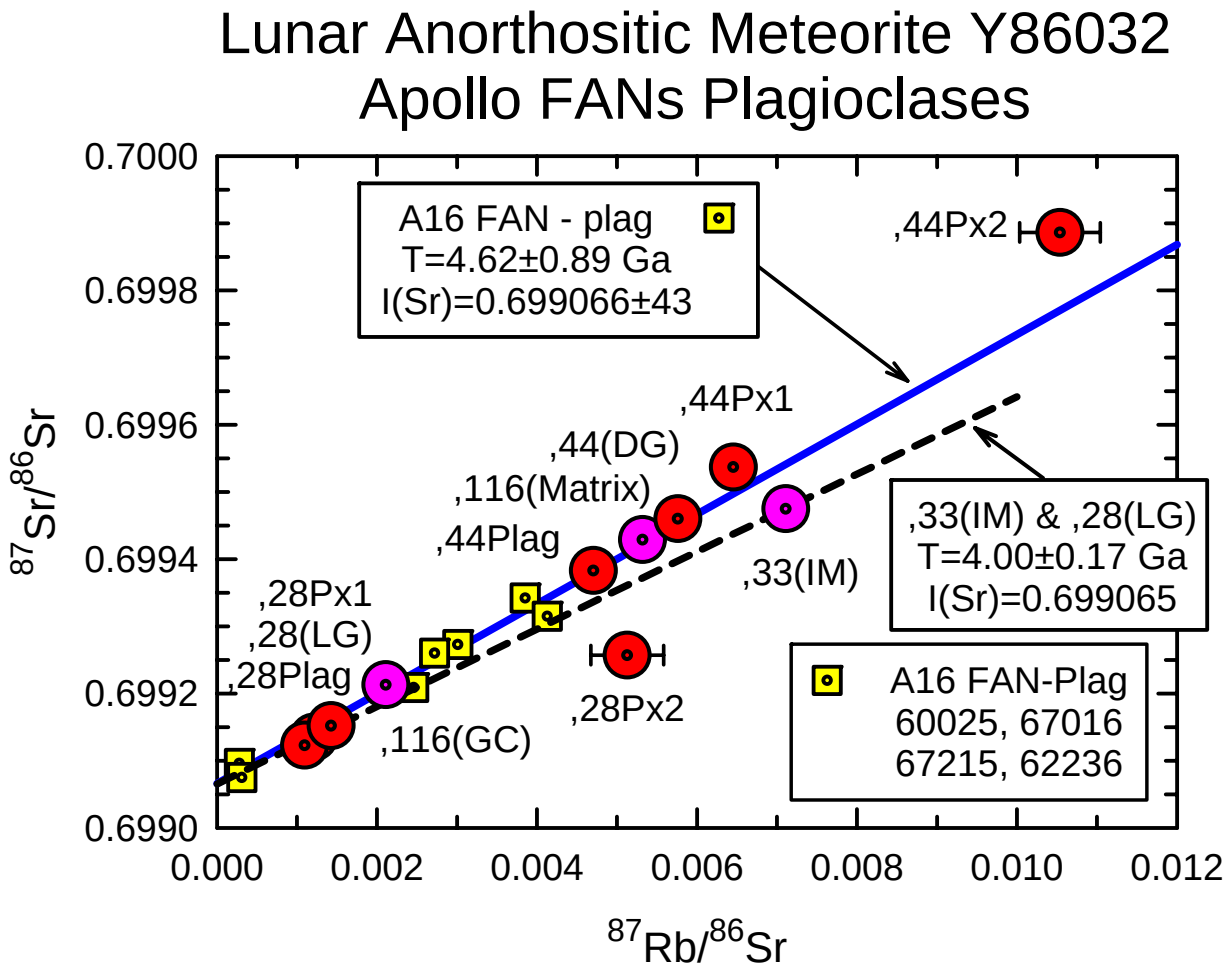

Figure 10

Nyquist et al.

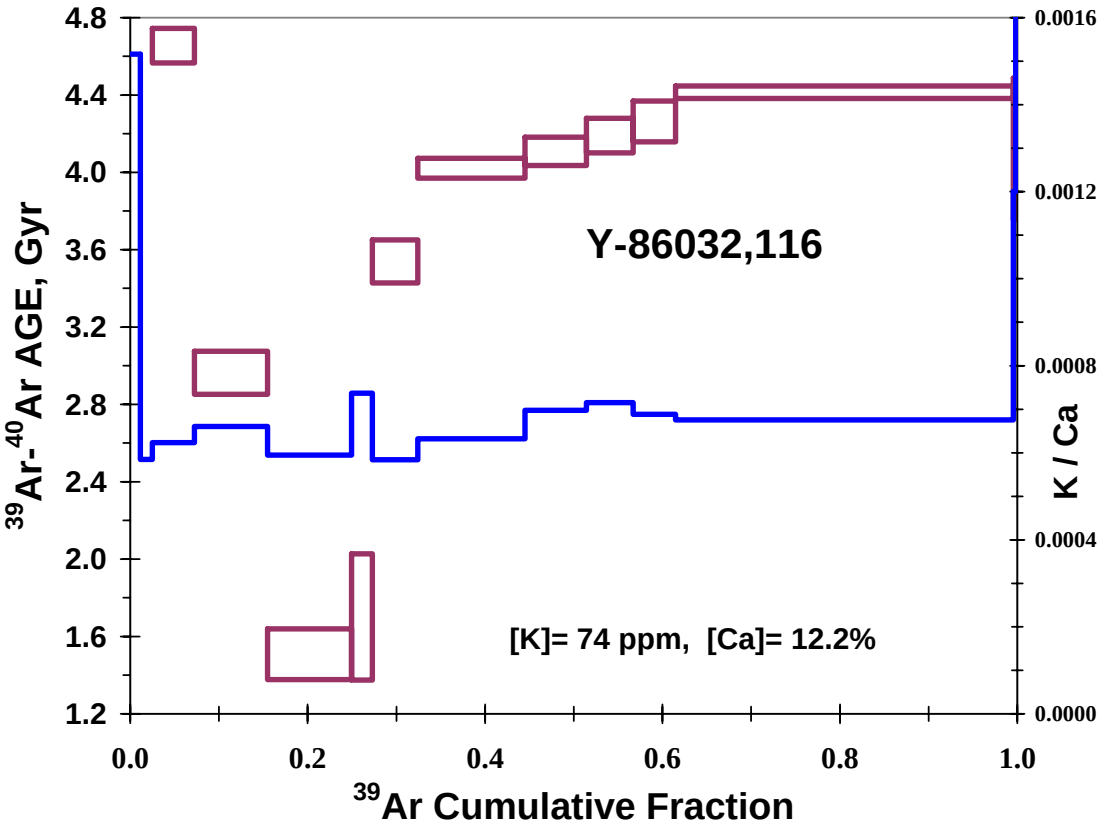

Figure 11

Nyquist et al.

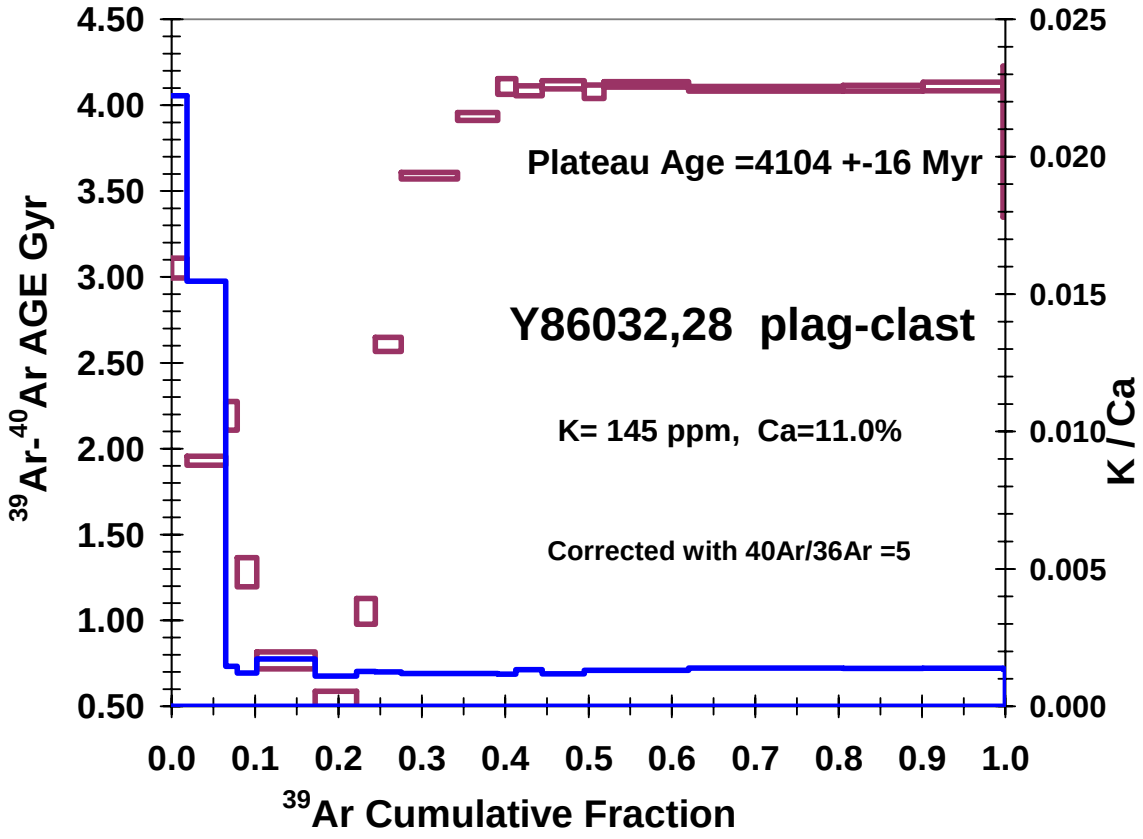

Figure 12

Nyquist et al.

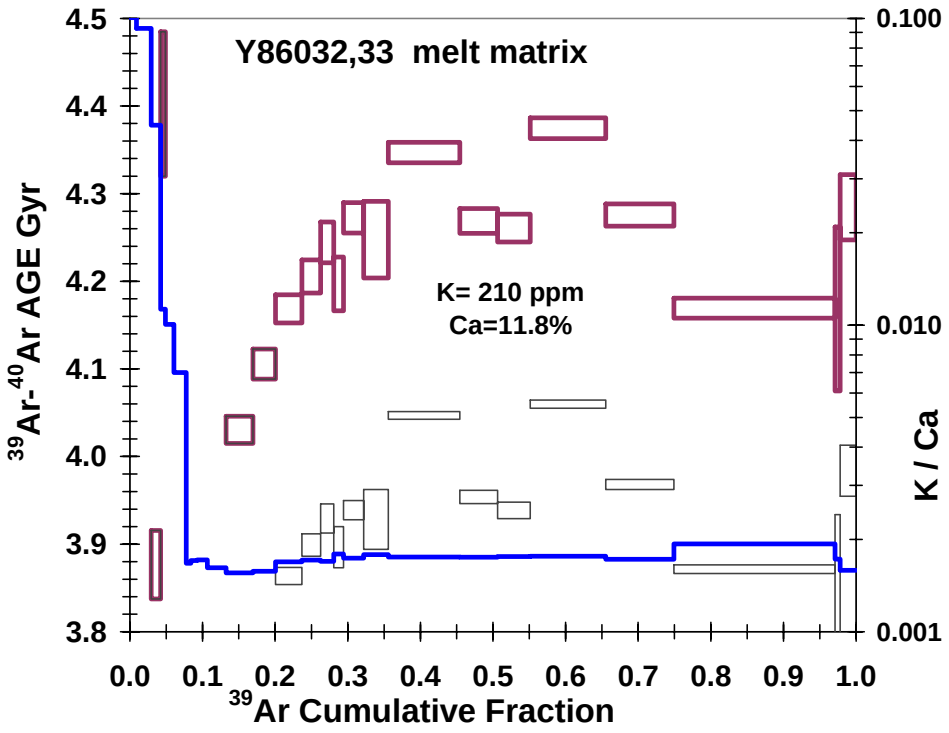

Fig. 13

Nyquist et al.

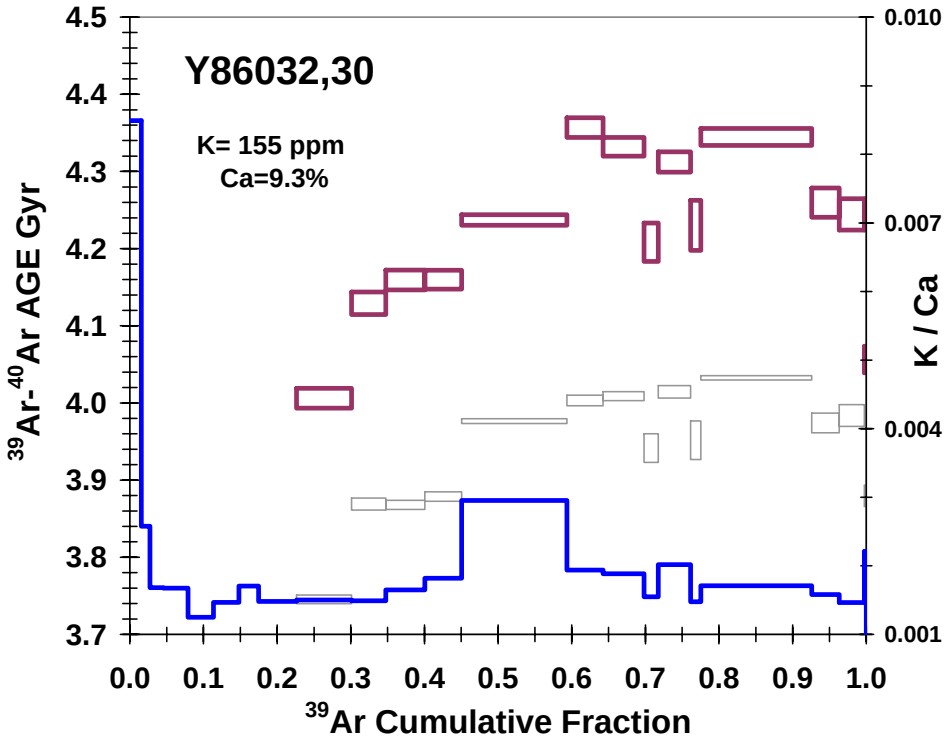

Fig. 14

Nyquist et al.

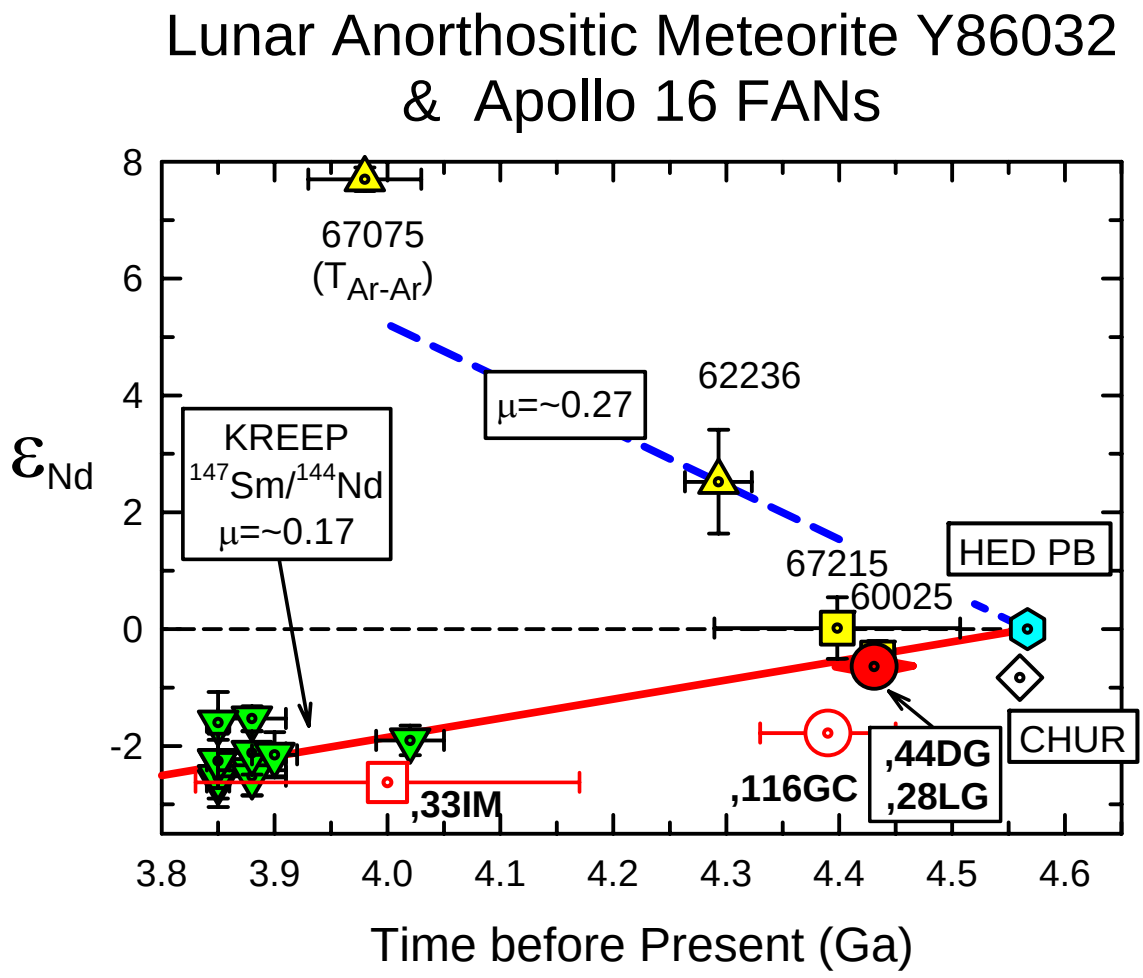

Fig. 15

Nyquist et al.

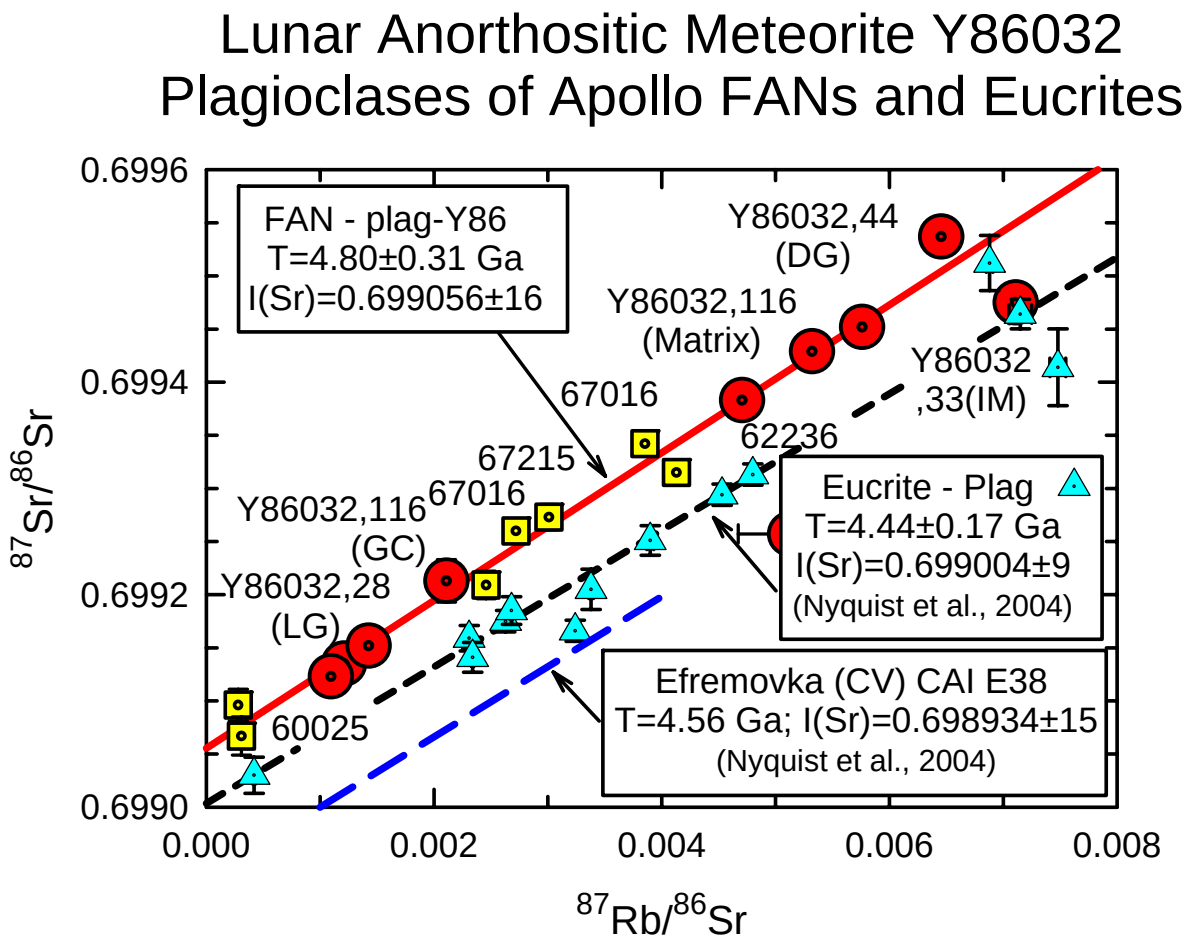

Fig. 16

Nyquist et al.